**Ivan Aristides Ferreira Garcia**

Licenciado em Engenharia Civil

# $VO_2$ thin films and nanoparticles for energy-saving applications in architectural elements

Dissertação para obtenção do Grau de Mestre em
Energias Renováveis: Conversão Elétrica e Utilização Sustentável

Orientador: Luís Miguel Nunes Pereira, Prof. Auxiliar, FCT-UNL
Co-orientador: Anabela Gonçalves Pronto, Prof. Doutora, FCT-UNL

Júri:

Presidente: Doutor Mário Fernando da Silva Ventim Neves, FCT/UNL
Arguente: Hugo Manuel Brito Águas, FCT/UNL

**Novembro de 2015**

# FILMES FINOS TERMOCRÓMICOS PARA APLICAÇÃO NA EFICIÊNCIA ENERGÉTICA DE EDIFÍCIOS



Faculdade de Ciências e Tecnologia

Universidade Nova de Lisboa

## ACKNOWLEDGEMENTS

Esta dissertação representa o pináculo da minha carreira académica, até à data. Uma carreira com altos e baixos, mudanças improváveis e surpresas memoráveis, mas sempre com uma forte vontade de sucesso.

Como autor desta dissertação, eu acredito vivamente que a colaboração e cooperação conduziram-me a um desempenho mais elevado e a melhores resultados. Por isso, sinto-me encorajado a mencionar as pessoas que, de uma forma ou de outra, me ajudaram a chegar tão longe na minha vida:

O meu orientador, Luís Pereira, cuja ajuda e conselhos provaram ser indispensáveis através deste trabalho. Ao mostrar o seu interesse contínuo no nosso trabalho, encorajou-me a trabalhar melhor. Estou sinceramente agradecido pela oportunidade que me deu ao trabalhar neste projeto.

A minha colega e amiga, Inês Cunha. É seguro dizer que sem a ajuda e conselhos da Inês, não teria, de todo, chegado até aqui. O seu otimismo, paciência e grande ajuda deram-me um valioso contributo para compreender parte de conhecimentos totalmente novos para mim, relacionados com Engenharia de Materiais. Obrigado pela paciência e colaboração durante todo o projeto.

O meu colega e amigo, José "Zeca" Gonçalves. O seu grande otimismo, confiança e amizade ajudaram-me, indiretamente, a nunca desistir perante nenhum problema. Embora tivéssemos trabalhos muito diferentes, a nossa cooperação impulsionou-os significativamente a níveis mais elevados.

O meu grande amigo de longa data, Gabriel Martins. Por me ajudar a encontrar pessoas que me pudessem ajudar a compreender e resolver problemas inerentes a este trabalho. Contudo, o seu maior contributo foi fazer parte de muitos momentos para relaxar a mente e recarregar baterias para mais um dia de trabalho. Os nossos jantares semanais adicionaram energias positivas a cada semana.

Os meus colegas de trabalho, Alexandra Gonçalves, Carolina Marques, Diana Gaspar, Joana Pinto, Raquel Barras, Ricardo Ferreira, Sónia Pereira e Tiago Carvalho pela assistência amigável, sugestões e colaboração neste trabalho.

Os dois colegas franceses, Aloïs Erker e Romain Gonçalves. A ajuda prática em laboratório e na construção dos modelos das casas impulsionaram significativamente o progresso do trabalho.

A minha co-orientadora, Anabela Pronto. As suas sugestões mostraram novas portas a explorar a longo prazo.

Dr. Russel Binions. O apoio amigável e sugestões ajudaram a procurar soluções para problemas complexos.

A minha sempre presente família, em especial a minha avó. Graças às suas refeições preparadas cuidadosamente, pude manter-me física e mentalmente saudável durante todo o semestre.

A minha Claudocas. Pelos bons momentos que passamos juntos e pela motivação a atingir patamares superiores. Um obrigado e um beijinho muito especial ☺

Um agradecimento, também, ao CTCV - *Centro Tecnológico da Cerâmica e do Vidro* e à Glexyz. Em particular, ao Dr. Hélio Jorge e ao Eng.º Tiago Fernandes pela colaboração prestada neste trabalho.

Sinto-me orgulhoso por ter tido a oportunidade de conhecer pessoas de grande valor neste percurso, até aqui. Sendo o futuro incerto e imprevisível, resta-me desejar a todos os que contribuíram para este trabalho memorável, os meus sinceros agradecimentos e votos para que seja tão pleno de sucesso e bons momentos, tal como o desejo para mim.

## ABSTRACT

Vanadium dioxide ($VO_2$) is a promising material with large interest in construction industry and architecture, due to its thermochromic properties. This material may be used to create "smart" coatings that result in improvements in the buildings energy efficiency, by reducing heat exchanges and, consequently, the need for acclimatization. In this work, $VO_2$ thin films and coatings were produced and tested in laboratory, to apply in architectural elements, such as glass, rooftop tiles and exterior paints. Thin films were produced by RF magnetron sputtering and $VO_2$ nanoparticles were obtained through hydrothermal synthesis, aiming to create "smart" windows and tiles, respectively. These coatings have demonstrated the capability to modulate the transmittance of infrared radiation by around 20%. The $VO_2$ nanoparticle coatings were successfully applied on ceramic tiles. The critical temperature was reduced to around 40ºC by tungsten doping. Ultimately, two identical house models were built, in order to test the $VO_2$ coatings, in real atmospheric conditions during one of the hottest months of the year, in Portugal – August.



**Keywords:** vanadium oxide ($VO_2$); thin films; smart tiles; energy efficiency; thermochromism; RF sputtering.

## RESUMO

O dióxido de vanádio (VO2) é um material promissor com grande interesse na indústria da construção e arquitetura, devido às suas propriedades termocrómicas. Este material pode ser usado para criar revestimentos "inteligentes" que resultam em melhorias na eficiência energética de edifícios, ao reduzir trocas de calor e, consequentemente, a necessidade de climatização. Neste trabalho foram produzidos e estudados filmes finos e revestimentos de $VO_2$, em laboratório, para aplicar em elementos arquitetónicos, como vidro, telhas e tintas exteriores. Os filmes finos foram produzidos por pulverização catódica (sputtering) assistida por magnetrão e as nano partículas de $VO_2$ foram obtidas por síntese hidrotermal, com o objetivo de criar janelas e telhas "inteligentes", respetivamente. Estes revestimentos demonstraram a capacidade de modular a reflectância de radiação infravermelha em cerca de 20%. Os revestimentos de nano partículas de VO2 foram aplicados com sucesso sobre telhas cerâmicas. A temperatura crítica foi reduzida para cerca de 40 °C, através da dopagem com tungsténio (W). Em última análise, foram construídos dois modelos de casas idênticos, com o objetivo de testar estes revestimentos em condições atmosféricas reais durante um dos meses mais quentes do ano, em Portugal – agosto.



**Palavras – Chave**: óxido de vanádio ($VO_2$); filmes finos; eficiência energética; termocromismo, pulverização catódica, telhas inteligentes.

# INDEX

## FIGURE INDEX

## TABLE INDEX

## LIST OF ABREVIATIONS

CEMOP/UNINOVA – *Centro de Excelência de Microelectrónica e Optoelectrónica e de Processos*
CENIMAT/I3N – *Centro de Investigação de Materiais/ Instituto de Nanoestruturas, Nanomodelação e Nanofabricação*
cm – Centimeter
CTCV – Centro Tecnológico da Cerâmica e do Vidro
CVD – Chemical vapor deposition
DC – Direct current
DP – Deposition pressure
EC – Electrochromic
H – Hour
IR – Infrared
mbar – milibar
min – minute
NIR – Near-infrared
$N_2$ - nitrogen
Pdep – Deposition pressure
PVD – Physical vapor deposition
RAC – real atmospheric conditions
RF – Radiofrequency
Rpm – Rotations per minute
RT – Room temperature
sccm – standard cubic centimeter per minute
SEM – Scanning electron microscope
ST – "smart" tile
$T_c$ – Critical temperature
TC – Thermochromic
UV – Ultra-violet
$V_2O_5$ – Vanadium pentoxide
VC – Vacuum chamber
Vis – Visible
$VO_2$ – Vanadium dioxide (IV)
$VO_x$ – Vanadium oxide
$WO_3$ – Tungsten oxide
XRD – X-Ray diffraction

### GREEK SYMBOLS

$\lambda$ – Incident wavelength [nm]
$\theta$ – Angle between the incident radiation and the studied plan

# 1. INTRODUCTION

In this chapter, it is introduced the main subject, motivations and objectives of this dissertation.

## 1.1 Motivation and objectives

Due to modern societies' thirst for energy, it is of upmost importance to discover, optimize and implement ways of reducing the need for more energy demand. Throughout History, technology has always taken part in Humanity's needs for harvesting different types of energy supplies. In the modern world, most of the energy that is consumed worldwide comes from primary sources like fossil fuels, namely coal and petroleum as the most-used of them. Besides being classified as finite primary resources, their burning and refining for producing secondary forms of energy, like electricity, releases greenhouse gases. These gases rise the levels of air pollution, massively concentrated in large metropolis, and contribute for the aggravation of the global warming.

Renewable sources of energy, like the Sun and the wind are becoming more used and reliable for harvesting. Also, their exploration does not contribute to the increase of greenhouse gases. State-of-the-art equipment and environmental-friendly policies are transforming the energy paradigm all over the planet. Unfortunately, the pace of which it is being done is still very slow. Though it is of common knowledge that global warming is a reality – and Man is probably its greatest catalyzer – scientists, engineers and academics are struggling to find new forms of reducing our "hunger" for energy.

Bringing together three distinct areas – Civil Engineering, Renewable Energies and Materials Engineering – was a unique opportunity to envision and work on something that could certainly make a difference, a common goal: improve energy efficiency in buildings.

The transportation, industrial and domestic sectors are the big hitters when talking about energy requirements. In the domestic and service sectors, it can be found that buildings air conditioning systems, for example, represent an average of 25% to 40%, respectively, of its total energy costs [1] ,[2]. These are values valid only for the developed countries. There are effective forms of reducing this value, either active or passive. An active form, for example, could be the replacement of old electrical equipment for more efficient ones. One of the forms to passively reduce air conditioning needs inside a building is to improve architectural elements to reduce heat gain. Double glass windows are a simple example that improve the thermal behavior of these elements. Regardless of the many construction elements a building has, windows and other glass elements represent an important part in a building's envelope.

Thermochromic (TC) materials are being studied for decades for their interesting temperature-sensitive properties. These materials shift their optical properties according to temperature changes, as they can alter their physical structure. Optical properties are also altered, leading in some cases to interesting reactions like the reflection of different parts of the solar spectrum. This alteration is interesting to apply in "smart" windows. To further understand if these properties can significantly improve a building energy-saving behavior, we were driven to take on this study. The thermochromic material used in this work was $VO_2$. An effort was made to co-relate standard deposition conditions with its structural and morphological properties, in order to optimize its optical properties.

In this work, besides the application in windows, the application of this technology was tested on roof-tiles. Since there is not much bibliography regarding this issue, we found it also interesting to include. Two house models were made to test the applicability of $VO_2$ layers on roof-tiles, in real life conditions.

$VO_2$ layers were obtained from nanoparticles based films and physical vapor deposition (PVD), in laboratory, in CEMOP/CENIMAT. Furthermore, they were analyzed and characterized in CENIMAT.

## 1.2 Structure of the dissertation

This work follows the below structure:

**Chapter 1** – Introduction to the main subject, motivations and objectives of this dissertation.

**Chapter 2** – A brief revision of the state-of-the-art of the main technologies used during this work.

**Chapter 3** – Production and characterization techniques are explained.

**Chapter 4** – Experimental procedures and results are explained in detail.

**Chapter 5** – Conclusions and future work perspectives.

**Chapter 6** – Bibliography and references.

**Annex –** Contains complementary data.

## 1.3 Original contributions

The major innovative contribution of this work is the experimentation of "smart" tiles in two identical house models, exposed to real atmospheric conditions (RAC), with temperature sensors installed. These sensors acquired data from the exterior temperature, as well as the interior of each model, allowing to make a precise comparison between both models data.

It was the first time such procedure was made, with no reports being found about it, elsewhere. The main objective was to obtain data of the $VO_2$ coatings in real conditions, as approximate as it could be in a real-scaled house, and compare the results, concluding if the "smart" coatings efficiently reduced the interior temperature of the correspondent model, reducing the need for acclimatization, or not. Although, the models were built specifically for the purpose of this work, the possibility of re-using them for future works is also available.

# 2. STATE-OF-THE-ART

In this chapter, it is presented a brief revision of the state-of-the-art of the main technologies used during this work.

## 2.1 Energy efficiency in buildings

There are different ways to improve the buildings' energy efficiency. The most obvious is directly related to architecture design. Factors such as the building solar orientation, number and size of windows and doors, construction materials and roof-type choices, greatly influence its energy consumption rate, whether for lighting and heating/cooling [3], [2]. Another important way of improving it is through passive solutions [4], [5].

Examples of passive techniques can be the use of natural ventilation, reduced solar gain in the summer through shadowing, use of vegetation to reduce heat gain (Fig. 2.1) or application of innovative technological materials for the same effect [1], [6]. It is in this latter technique that this work is located.

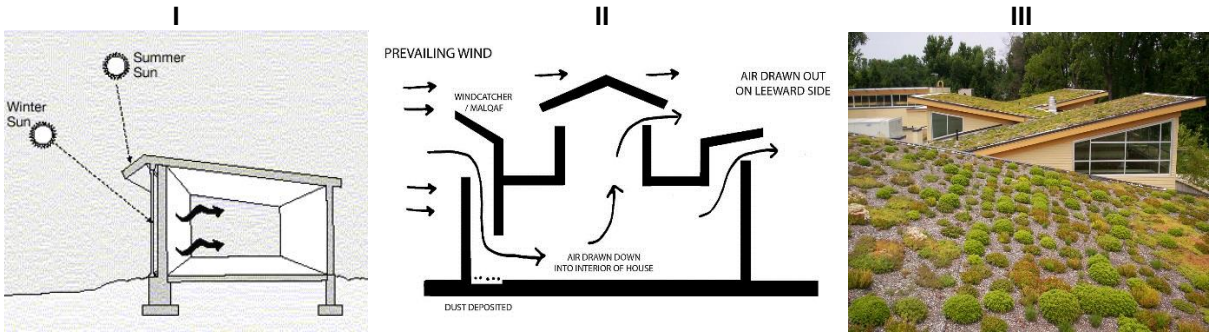


**Figure 2.1 - Passive solutions to improve energy efficiency: I - Trombe Wall; II - Natural ventilation; III - Green roofs** [7]–[9]**.**

During this work, the effect of a well-known thermochromic material, vanadium dioxide ($VO_2$), was studied on elements of a small scale house.

## 2.2 Chromogenic materials

Chromogenic materials are known to alter their optical properties according to an external stimulus [10]. In Table 2.1, it can be seen some of their variations:

**Table 2.1 - Chromogenic technologies and their respective stimuli** [10]

| Technology | Stimulus required |
|---|---|
| Thermochromic | Temperature |
| Electrochromic | Potential difference |
| Photochromic | Light irradiation |
| Gasochromic | Exposure to reducing/oxidizing gases |
| Piezochromic | Mechanical pressure |

In the pictures below can be seen examples of chromogenic technologies.

Thermochromic Electrochromic Photochromic

**Figure 2.2 – Examples of different types of chromogenic technologies** [11][12][13]**.**

When thinking about which chromogenic materials have the highest interest to apply in architectural elements, such as windows, it is clear which of these stand out: thermochromic (TC), electrochromic (EC) and photochromic (PC) (Fig. 2.2).

In order to improve the energy efficiency of buildings, an obvious point to look at is their weak points – windows. They represent an important link between the interior and exterior of the building, as well as providing natural light for the comfort of their occupants. Nevertheless, a normal window can have thermal losses of nearly 1 $W/m^2K$ [14].

Granqvist *et al.* concluded in a recent study that chromogenic technology is proving to be effective against energy waste in buildings:

> *"(…) research, development, and industrialization of chromogenic technologies progress at a healthy pace and give prospects for buildings which are less wasteful with regard to energy at the same time as they are more comfortable for their users."*[10]

## 2.3 Thermochromics

TC materials are known for changing their optical and electrical properties according to temperature. Transmittance and reflectivity may vary significantly when reaching "critical" temperatures, Tc [10]. These temperatures correspond to the reversible transition phase from an insulator or semi-conducting state to a metallic state.

When looking at a clear-glass window, for example, transmittance can be put simply as the total radiation that passes through the window, whereas reflectivity is the amount of radiation that is reflected from the surface. Below Tc, a TC coating is infrared transparent. In a smart window with a $VO_2$ thin film coating above Tc, it can reflect most of the near-infrared radiation from the surface. In Fig. 2.3 is shown a representation of the previous example.

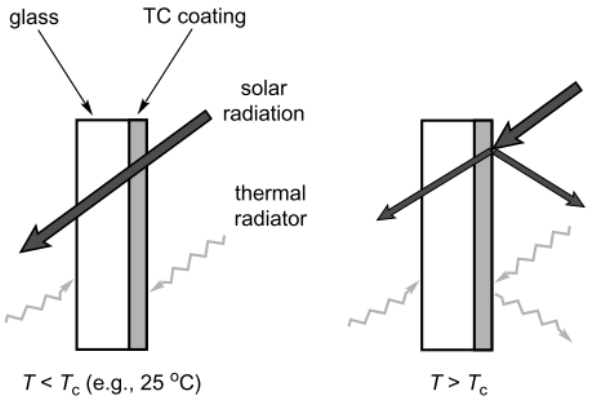


**Figure 2.3 - Representation of a smart window with a TC coating** [15]**.**

The same principle can be applied to a single roof tile (Fig. 2.4). In this work, the surface of several roof tiles was covered with $VO_2$ nanoparticles, in order to coat an entire roof with "smart" tiles (ST).

When compared to the application in windows, the tile coating is less limited. Since the layers are to be deposited onto an opaque surface, the need for a semi-transparent coating is unnecessary. However, in the case of nearly black $VO_2$ layers, the coated tile will absorb more radiation until it reaches the Tc. Therefore, it can lead to higher temperatures on the roof, when compared to a normal roof. This effect is also studied further in this work.

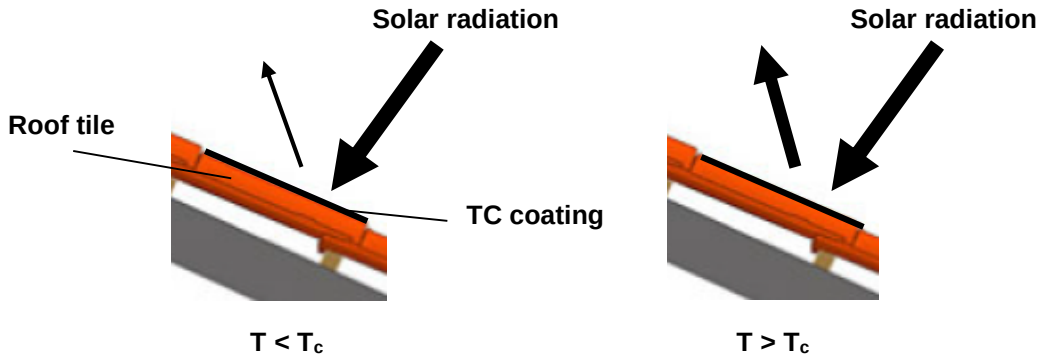


**Figure 2.4 - Representation of a "smart" tile with TC coating.**

There are several TC compounds, such as $Fe_3O_4$, $NbO_2$, NiS, $Ti_2O_3$, $VO_2$ and $V_2O_5$ [16]. The most commonly studied are $VO_2$ and vanadium pentoxide ($V_2O_5$), for their multiple properties and lower transition temperatures. Both change their optical properties – transmittance and reflectivity – when they reach "critical" temperatures, $T_c$ [10]. $V_2O_5$ has a higher $T_c$ and is studied for its thermoelectric characteristics and electro-optical properties [17], [18]. $VO_2$ is particularly more interesting due to having the lowest $T_c$ – 68 ºC. Moreover, it is possible to lower it even more by doping with other elements, such as tungsten oxide ($WO_3$). This process will be discussed later. Table 2.2 shows the different values of $T_c$ of both phases in their bulk-like form.

**Table 2.2 - Vanadium oxide phase vs. critical temperature**[19]

| Vanadium oxide phase | Critical Temperature (ºC), $T_c$ |
|---|---|
| $VO_2$ | 68 |
| $V_2O_5$ | 250 |

### 2.3.1 Vanadium oxide

Vanadium oxide has been continuously studied for its thermochromic properties. From the previous phases of $VO_x$ shown, it is obvious that $VO_2$ stands out for its lower transition phase temperature (68 ºC). At temperatures below $T_c$, it is monoclinic, semi-conducting and transparent to most of the infrared radiation. At temperatures above $T_c$, its electrical conductivity rises significantly and it is followed by an increase in infrared reflectivity [20]. Its molecular structure also changes to metal-like (tetragonal), as shown in Fig. 2.6. The tetragonal metallic structure is responsible for the partial infrared reflection, due to the existence of free electrons, which increases its conductivity.

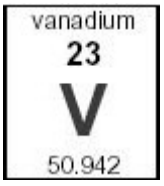


**Figure 2.5 - Vanadium**

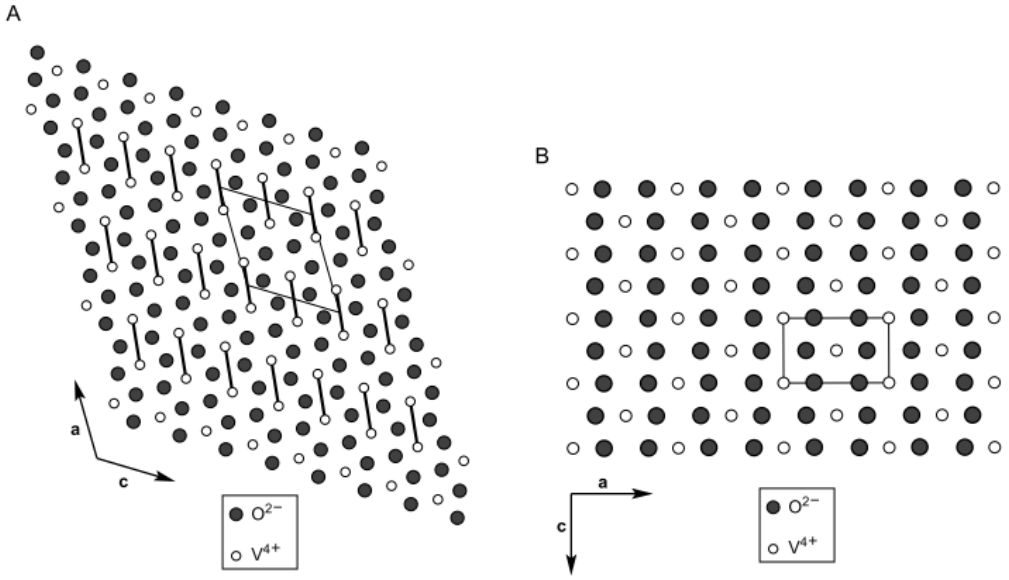


**Figure 2.6 - Representation of monoclinic structure (A) and tetragonal structure (B) of $VO_2$ [15].**

Even by having the lowest $T_c$ of the thirteen $VO_x$ phases known[19], $VO_2$ critical temperature is still relatively high comparing to the average ambient temperature of 25 ºC.

### 2.3.1.1 $VO_2$ doping

As seen in Table 2.2, the bulk-like form of $VO_2$ has a $T_c$ approximately of 68 ºC. From the buildings' perspective, it is necessary to lower that value closer to the average room temperature, 25 ºC. The transition phase temperature can be lowered by doping the solution with another element. There are different elements that can be used for this process, namely tungsten (W), niobium (Nb) and titanium (Ti). So far, W has proved to be the most effective dopant for reducing $T_c$ of $VO_2$ thin films by more than 20 ºC [20].

One of the problems regarding "smart" windows TC coating is the reduced amount of visible light transmittance. On the one hand, TC coatings reduce the amount of energy required for cooling, which will improve the buildings' energy efficiency. On the other hand, additional lighting energy will be needed, re-balancing the energy balance.

Granqvist *et al*. published in 2009, results of 45% luminous transmittance above $T_c$ for single-layer thin films. In their study, single-layer films showed lesser values of transmittance when compared to multi-layer ($TiO_2/VO_2/TiO_2$) results of 58% [21]. Zhang *et al*. affirmed, in 2010, that the visible transmittance needed for comfortable architectural glazing should exceed 60%. However, reports of only 55% transmittance have been achieved using fluorine (F) as dopant for single-layer films [22][23].

Another problem related to TC thin films is their unpleasant brownish color. Architectural concepts demand that window coatings should be as clear and pleasant as possible to provide the most of natural lighting and visual comfort. In 2009, Saeli *et al*. reported that the inclusion of gold (Au) nanoparticles in the films matrix would change the brown color of the glass coatings to a range of blue and green pigmentation, depending on the concentration of Au/V. In Fig. 2.7 we can observe their results:

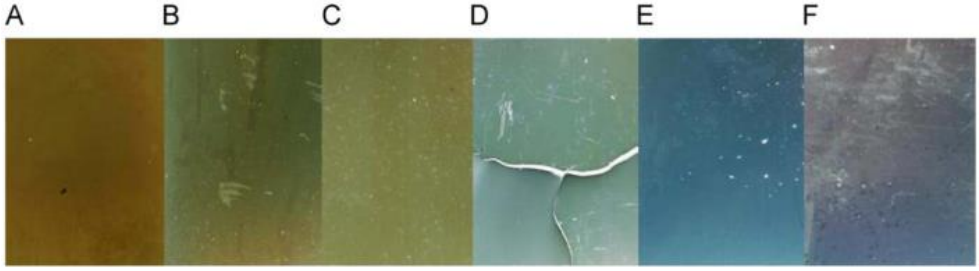


**Figure 2.7 - Examples of glass with gold and vanadium dioxide nano-composite films. The films had a Au/V ratio of: (A) 0 (W-doped $VO_2$), (B) 0.09 (C) 0.15, (D) 0.30, (E) 0.36 and (F) ∞ (gold nanoparticle film)** [24].

More recently, Sun et al presented a method to transform vanadium pentoxide ($V_2O_5$) into $VO_2$ sculptured thin films, with superior thermochromic properties.[25]

### 2.3.2 Solar radiation

The solar radiation that hits the surface of the Earth is made of three distinct zones of the spectrum – ultra-violet (UV), visible and infrared (IR) radiation. Each zone has a different range of wavelength. Fig. 2.8 shows the representation of the solar spectrum:

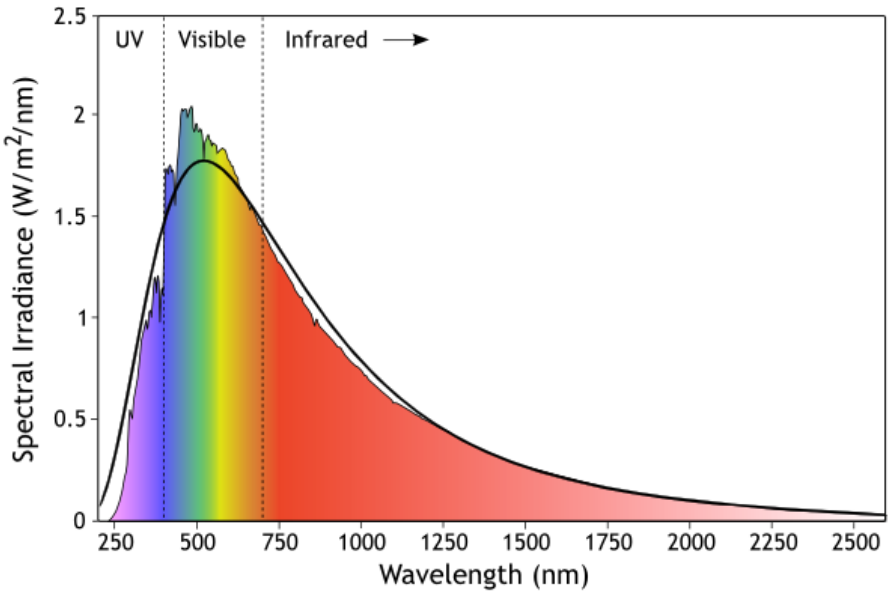


**Figure 2.8 - Representation of the solar spectrum** [26]**.**

Most of the spectral irradiance is represented by infrared, close to 50%, which is also responsible for heating. Thermochromic materials, such as $VO_2$, are known for their capacity of reflecting IR radiation when they reach temperatures above $T_c$ [21].

During this work, we focused mainly in the capacity of a $VO_2$ thin film to reflect near-infrared (NIR) and visible radiation, leaving the ultra-violet (UV) as a recommendation for future works.

# 3. PRODUCTION AND CHARACTERIZATION TECHNIQUES

In this chapter, it is explained the methods and techniques used in order to produce and characterize $VO_2$ thin films.

## 3.1 $VO_2$ production

The production of single crystals of $VO_2$ are unpractical for many technological applications mentioned before. The stresses caused by phase transition are known to crack them after a few cycles, affecting conductivity. Thin films, however, can handle those stresses excellently, with reports showing that they can be cycled $10^8$ times without losing any electrical contrast [15].

The films produced during this work were made using a commercial $VO_2$ target (Alineason, 99.99% pure). In parallel, $VO_2$ powder was produced in laboratory to apply on tiles and paints. This process will be described in detail, further in this work.

## 3.2 Deposition techniques

There are various processes of thin films deposition. Below, are listed and shortly described the ones most used worldwide [20]:

**Sol gel**: It has been widely used since the early 1980s. It involves the hydrolysis of the initial coating in order to obtain crystalline $VO_2$.

**Physical vapor deposition** (PVD): This is a general term which includes:

- **RF magnetron sputtering**: Technique used in this work, therefore it will be explained further.
- **DC magnetron sputtering**: Similar to the above. Uses a direct current magnetron to produce thin films.
- **Pulsed laser deposition**: Laser ablation technique developed for the deposition of thermochromic thin films. It has also been used for the investigation of composite materials.
- **Atomic layer deposition**: Used for the fabrication of ultra-thin films.

**Chemical vapor deposition** (CVD): A term that refers to similar techniques. This method basically uses organometallic precursors at low pressure conditions and includes:

- **Atmospheric pressure chemical vapor deposition** (APCVD): This method allows controlled isolations of VO states and occurs at atmospheric pressure. VOx thin films produced show rich concentrations of oxygen.
- **Aerosol assisted chemical vapor deposition** (AACVD): In this process, the precursor is dissolved into a solvent. Thereafter, an aerosol is generated to complete the process. Unlike APCVD, this technique doesn't require a volatile precursor.

Furthermore, hydrothermal synthesis was used to obtain $VO_2$ micro and nanoparticles and used spray-coating to deposit them onto ceramic tiles surface [27], [28]. This technique will be explained later.

### 3.2.1 Physical vapor deposition

This method consists basically on three steps: evaporation/ejection, transportation and deposition. The material to be deposited, which in this work was $VO_2$, is known as the target and it is in

solid state. Afterwards, a high-energy beam of electrons or ions is generated by a power source and is directed towards the target under low pressure conditions. The atoms on the surface of the target are vaporized and will be gradually deposited on the substrates' surface, forming a thin film.

There are different methods to remove the atoms of the surface of the target. One of the most common, due to its effectiveness, is magnetron sputtering, where the high energy ions can be generated by a radio-frequency or DC (RF or DC magnetron sputtering, respectively).

#### 3.2.1.1 RF magnetron sputtering

In RF magnetron sputtering, an inert gas (normally argon) is ionized by the action of a radio-frequency voltage supplied by the power source, while a magnetic field confines the generated plasma near the cathode. The target is fixed to the cathode, which is bombarded by argon ions, causing the ejection of the atoms from the surface[29]. Fig. 3.1 illustrates the main principle of magnetron sputtering.

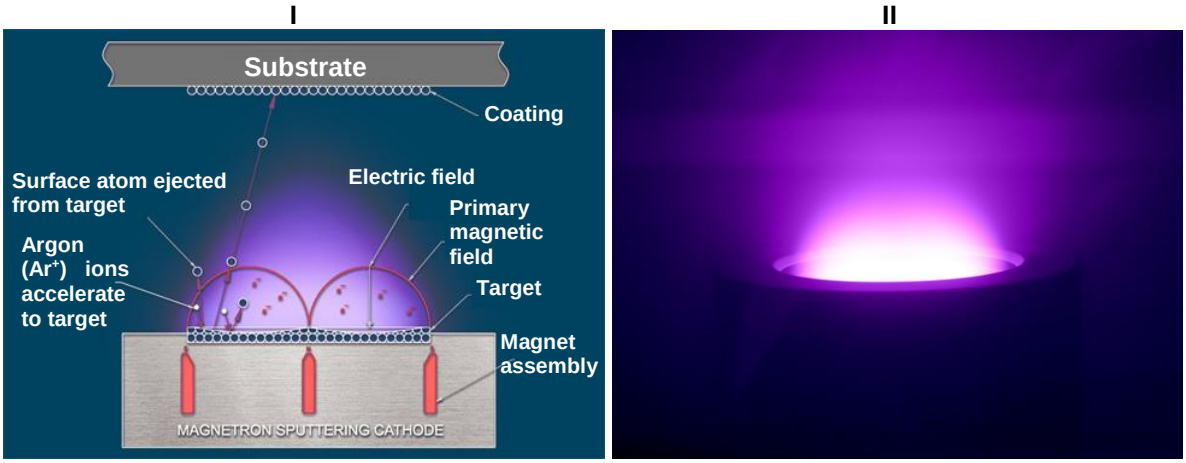


**Figure 3.1 – I) Magnetron sputtering principle, adapted** [30]**; II) Plasma over $VO_2$ target.**

The pressure system used in our work was a *Pfeiffer Vacuum Classic 500* (Fig. 3.2) located in CEMOP's laboratory.

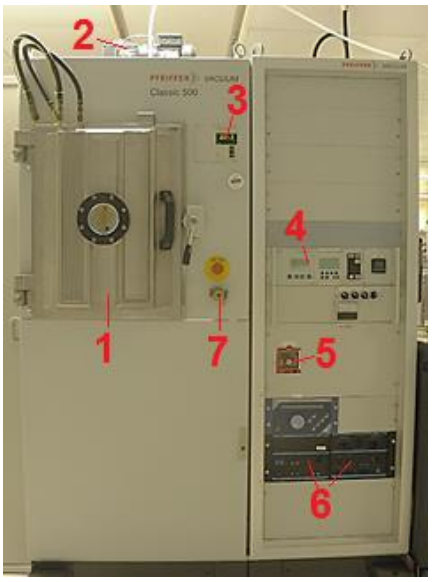


**Figure 3.2 – RF magnetron sputtering system: (1) Vacuum chamber; (2) Rotation pump; (3) Pressure display; (4) Pump control panel; (5) Samples rotation control; (6) RF magnetron control panel; (7) Air admission valve.**

During this process, an inert gas (Ar) is used to prevent chemical reactions between the target and the particles of the gas. A reactive gas, such as oxygen ($O_2$), may also be introduced in the sputtering process to change the properties of the films. This issue is also discussed further in this study.

#### 3.2.1.2 Co-sputtering

As the name suggests, co-sputtering is a technique used when it is necessary to have two or more targets simultaneously depositing onto a substrate. This is especially useful to dope thin films with another material. Two different targets are placed below the substrate, and controlled independently. While the deposition conditions are the same, since both are inside the VC, the power applied to each target can be controlled independently.

In this work, we used co-sputtering to dope $VO_2$ films with $WO_3$, in order to lower the thin films $T_c$.

**Figure 3.3 - Co-sputtering with $VO_2$ and $WO_3$.**

## 3.3 Characterization of the films

After the production of the films, it is necessary to study their properties, such as thickness, material structure, crystalline orientation, and even optical properties, such as transmittance and reflectivity. The characterization methods are introduced in this chapter and their results are showed in detail in chapter 4.

### 3.3.1 Profilometry

This technique is used to measure the thickness of the films. A profilometer is equipped with a needle with a highly sensitive diamond tip that slides over the surface of the sample, detecting elevations and depressions, at a nanoscale. The thickness of the films is obtained from the samples' profile. In this study, we painted small ink dots in the corners and center of each glass plate, to serve as "steps" to measure. The profilometer used in this experiment was an *Ambios XP-Plus 200 Stylus* (Fig. 3.4), located in CENIMAT.

1 2

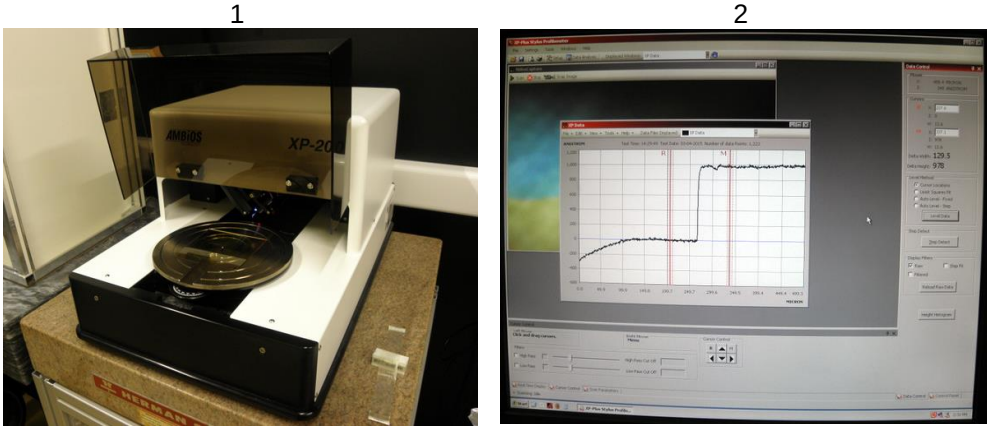

**Figure 3.4 -Profilometry equipment: (1) Profilometer *Ambios XP-Plus 200 Stylus*; (2) a sample profile.**

### 3.3.2 Sample cutting

The sample cutting was made using a glass scratcher (*Karl Suss HR 100*) (Fig. 3.5 (1)) in CEMOP's laboratory. The sample is placed on top of a rubber base, to maximize grip between the glass plate and the base. An angled diamond tip (Fig. 3.5 (2)) slides manually over the surface of the plate, in a straight line. A scratch on the glass is made, thus creating a weak breaking-point. Then, with the application of mechanical force, the glass should break by the weak line. This process can be repeated until the size of the sample is the desired.

1 2

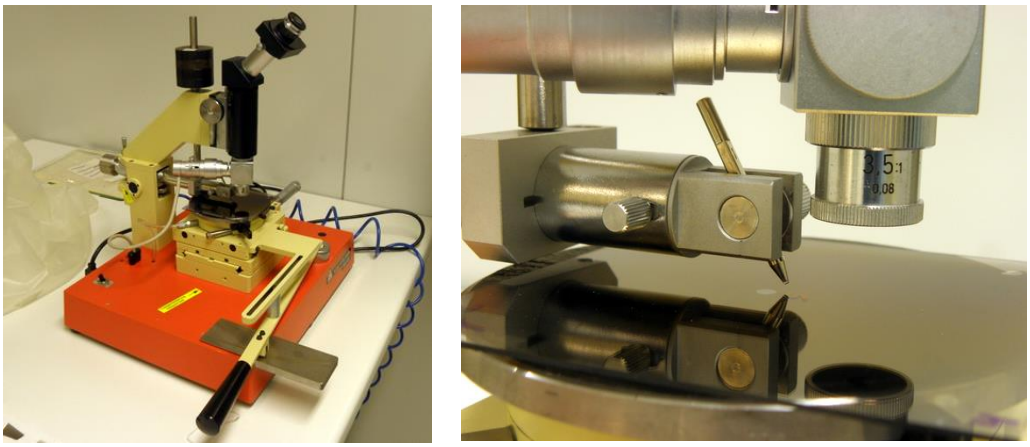

**Figure 3.5 - Glass cutting equipment, in CEMOP: (1) *Karl Suss HR 100*; (2) Cutter detail.**

### 3.3.3 Annealing

After the sputtering process, the samples' structure is amorphous. To form a crystalline structure, the samples have to be heat treated [31]. In order to analyze their physical properties by X-ray diffraction (XRD), it is necessary to have a monoclinic structure. To transform a sample's amorphous structure into monoclinic, it should be heated at a high temperature (+400 ºC), in a controlled-pressure environment. J. Livage showed that heating in air would lead to fully oxidized $V_2O_5$, whereas in a controlled-atmosphere under an inert gas ($N_2$), leads to an optically transparent and homogeneous $VO_2$ phase [31].

To perform the annealing of the samples, we used a laboratory furnace *ThermoLyne Tube Furnace 21100* (Fig.).

1 2

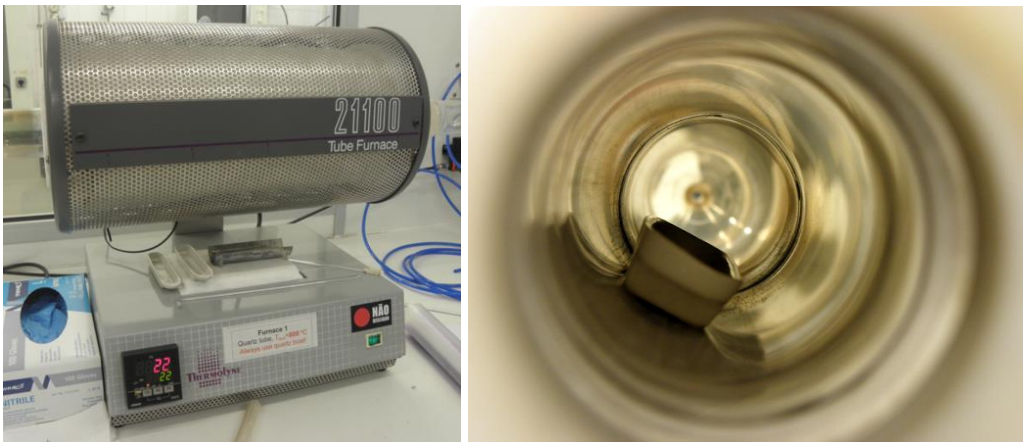


**Figure 3.6 – Laboratory tube furnace: (1) *ThermoLyne Tube Furnace 21100*. (2) Interior detail with samples.**

### 3.3.4 X-Ray diffraction

To analyze the samples' properties, such as crystalline orientation, average grain size or material structure, XRD can be used to obtain this data [32]. XRD analysis is required to determine whether the thin films produced are, in fact, $VO_2$ or a different VOx phase. Besides, it's a non-destructive technique for the identification and quantification of the crystalline phase of powdered and solid samples.

X-rays are created by the acceleration of electrons from a hot filament, to the anode material, in a HT tube. The x-ray beam hits the surface of the sample on an angled position and is refracted to a detector. The refracted ray is then analyzed according to Bragg's Law:

$$n\lambda = 2d \sin\theta \qquad (1)$$

Where $n$ is the reflection order, $\lambda$ is the incident wavelength, $d$ is the interplanar spacing and $\theta$ is the angle between the incident radiation and the studied plan [33]. This measures were conducted using an X-ray diffractometer *PANalytical X'Pert PRO MPD* (Fig. 3.7) in Lab 7, in CENIMAT.

**Figure 3.7 - *X-Ray diffractometer PANalytical X'Pert PRO MPD*.**

### 3.3.5 UV, visible and near-infrared spectroscopy

The UV-Vis-NIR spectroscopy is an important and non-destructive test, in which the sample's surface is exposed to a simulation of the solar spectrum. Relevant data, such as optical transmittance and reflectance are gathered and graphically analyzed. The spectrophotometer used in our work was a *PerkinElmer Lambda 950* (Fig. 3.8), in Lab 7.

1 2

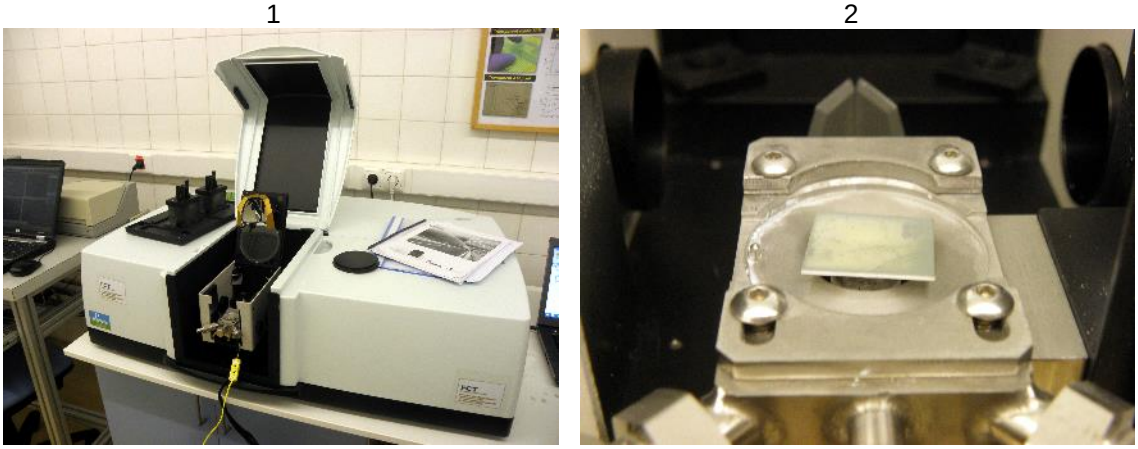

**Figure 3.8 - (1) Spectrophotometer *PerkinElmer Lambda 950*; (2) Sample detail.**

To control the sample's temperature, we used an integrated pyrometer, *Optex Thermo-Hunter*, with laser point.

# 4. EXPERIMENTAL PROCEDURES AND RESULTS

In this chapter, all the experimental procedures are explained in detail and follow a chronological order.

## 4.1 $VO_2$ thin films production by RF magnetron sputtering

This experiment took place in the laboratory of CEMOP. The main objective was to fabricate $VO_2$ thin films by RF magnetron sputtering, whilst optimizing the ideal conditions of **power**, **deposition pressure** and **$O_2$ flow**. For each condition were made three depositions.

In order to fabricate good quality thin films, it was used a commercial target of $VO_2$. Glass plates (10 cm x 10 cm, Marienfeld) were used as the deposition surface. The glass was ultrasonically cleaned with acetone and isopropanol before entering the vacuum chamber. The sputtering was always made at room temperature and the inert gas used was argon (Ar).


**Figure 4.1 - RF magnetron control panel: (1) Forward power; (2) Reflected power; (3) Reflected power tuning; (4) DC bias display; (5) Plasma indicator; (6) Power wheel.**

### 4.1.1 Power variation

To start the sputtering process, firstly, the deposition pressure, Ar flow and the pump's rotation were stabilized. With the deposition pressure stable at $4.0 \times 10^{-3}$ mbar, we switched on the RF magnetron, gradually raising the power to the desired level. To achieve the power required for the plasma build-up with the minimum losses, the reflected power should be ideally 0, or the closest to it possible. We made three depositions with the power set to 100 W, 125 W and 150 W. The deposition times were 40 min, 30 min and 20 min, respectively. In table 4.1, we can see the configuration settings for the three samples:

**Table 4.1 . Power variation settings**

| P (W) | T (min) | Pdep (mbar) | Ar (sccm) | $O_2$ (sccm) | DC Bias (V) | Pump speed (rpm) |
|---|---|---|---|---|---|---|
| 100 | 40 | $4.0 \times 10^{-3}$ | 35 | 0 | -228 | 21600 |
| 125 | 30 | $4.0 \times 10^{-3}$ | 35 | 0 | -251 | 21600 |
| 150 | 20 | $4.0 \times 10^{-3}$ | 35 | 0 | -278 | 21600 |

Settings:

- P – Power (W)
- T – Time (min)
- Pdep – Deposition pressure (mbar)
- Ar – Argon flow (sccm)
- $O_2$ – $O_2$ flow (sccm)
- DC Bias – DC Bias voltage (V)

- Rotation – Pump speed (rpm)

The first three samples (Fig. 4.2) were then removed and introduced new glass plates in the VC, for the next deposition.

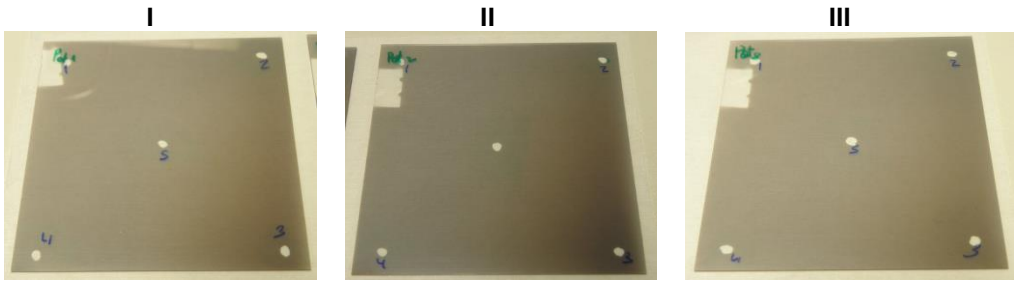


**Figure 4.2 - Power variation samples: I - 100 W, 40 min; II - 125 W, 30 min; III - 150 W, 20 min.**

As it can be seen in the images above (Fig. 4.2), all the samples present a grey color. The color gradient occurs due to the angled position of the substrate, relatively to the target. Moreover, the gradient suggests that darker pigmentation can represent greater film concentration.

### 4.1.2 Deposition pressure variation

The starting settings for this experiment were similar to the previous. This time, the condition to vary was the vacuum chamber's deposition pressure (DP). In order to change the DP, the Ar flow was changed. The power was set to 125 W and the time of each deposition was 30 min. In table 4.3 are the pressure deposition settings used:

**Table 4.2 – Deposition pressure settings**

| P (W) | T (min) | Pdep (mbar) | Ar (sccm) | $O_2$ (sccm) | DC Bias (V) | Pump speed (rpm) |
|---|---|---|---|---|---|---|
| 125 | 30 | $6.0x10^{-3}$ | 51 | 0 | -211 | 21600 |
| 125 | 30 | $8.0x10^{-3}$ | 68 | 0 | -198 | 21600 |
| 125 | 30 | $1.0x10^{-2}$ | 86 | 0 | -194 | 21600 |

The removal process was repeated and introduced the final set of glass plates.

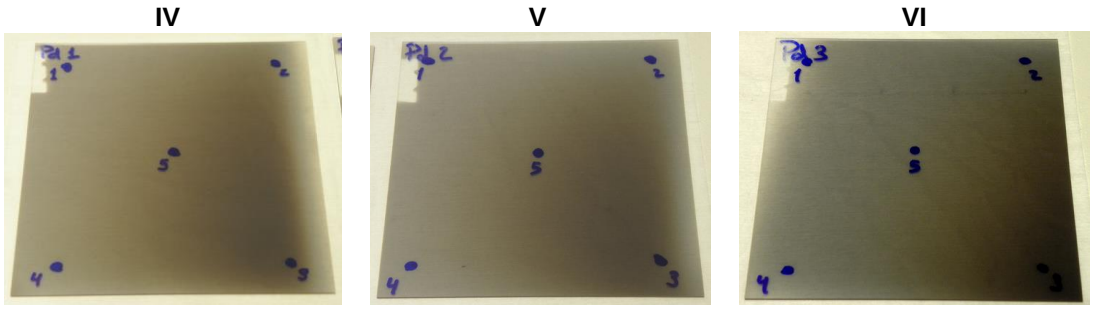


**Figure 4.3 - Pressure deposition samples: IV - 6.0E-3 mbar; V – 8.0E-3 mbar; VI – 1.0E-2 mbar.**

The new samples (Fig. 4.3) showed a darker color, compared to the previous set of samples. This effect was likely caused by the Ar flow increase, in the VC, which contributed to eject more atoms from the target, during the sputtering process. The gradient effect occurs due to the effect explained, previously.

### 4.1.3 O2 flow variation

The introduction of a reactive gas, such as $O_2$, in the sputtering process would alter the characteristics of the thin films deposited on the glass substrate. In this experiment it was introduced $O_2$, controlling its flow with a mass flow controller. To maintain the same flow of the first set of samples (35 sccm) in the gas chamber, the $O_2$ and Ar flowes were balanced. To keep the deposition pressure at 4.0E-3 mbar, it was necessary to adjust the pump's rotation. The settings used in the three depositions are represented in table 4.3:

**Table 4.3 - $O_2$ flow variation settings**

| P (W) | T (min) | Pdep (mbar) | Ar (sccm) | $O_2$ (sccm) | DC Bias (V) | Pump speed (rpm) |
|---|---|---|---|---|---|---|
| 125 | 30 | $4.0x10^{-3}$ | 34 | 1 | -240 | 18720 |
| 125 | 30 | $4.0x10^{-3}$ | 32,5 | 2,5 | -258 | 19800 |
| 125 | 30 | $4.0x10^{-3}$ | 30 | 5 | -289 | 24480 |

The final samples (Fig. 4.4) were removed and the sputtering experiment was terminated.

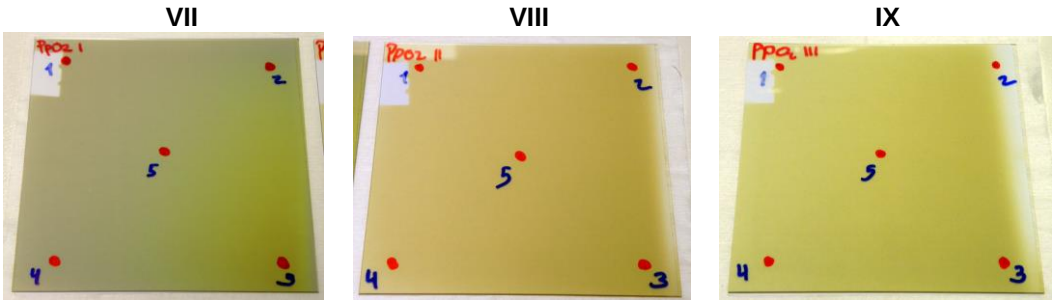


**Figure 4.4 - $O_2$ flow variation samples: VII – 1 sccm; VIII – 2.5 sccm; IX – 5 sccm.**

Contrary to the previous two sample sets, the new samples (Fig. 4.4) showed a yellow/green color. This has occurred by the oxidation of the $VO_2$ molecules, likely into $V_2O_5$.

### 4.1.4 $WO_3$ thin films production

In order to produce $VO_2$ thin films doped with $WO_3$ by co-sputtering, it was first necessary to analyze the growth rate of $WO_3$ layers deposited. For this experiment, we used the previous deposition system, varying only the power and we kept normal glass as the substrate. The parameters are shown in table 4.4:

**Table 4.4 - $WO_3$ deposition parameters**

| P (W) | T (min) | Pdep (mbar) | Ar (sccm) | $O_2$ (sccm) | DC Bias (V) | Pump speed (rpm) |
|---|---|---|---|---|---|---|
| 35 | 30 | $4.0x10^{-3}$ | 38 | 0 | -90 | 21600 |
| 50 | 30 | $4.0x10^{-3}$ | 38 | 0 | -106 | 21600 |
| 75 | 30 | $4.0x10^{-3}$ | 38 | 0 | -126 | 21600 |

Table 4.5 - $WO_3$ growth rates

| Sample | Growth rate (nm/min) |
|---|---|
| I – 35W | 3,4 |
| II – 50W | 3,8 |
| III – 75W | 5,1 |

The profilometry tests (Table 4.5) showed a higher growth rate with more power applied (75 W). With these results, to get $WO_3$ doping values of nearly 5% during co-sputtering, the power was optimized to 10W. The co-sputtering procedures and parameters can be seen later in this work, in sub-chapter 4.2.5.

## 4.2 Characterization results

The thin films produced by RF magnetron sputtering were characterized by different methods. The main purpose of their characterization was to obtain proper results and data regarding their composition and compare the samples' properties. It will be explained, in this sub-chapter, the methods used. Unless it is mentioned otherwise, all the experiments were made using CENIMAT's equipment and facilities.

### 4.2.1 Profilometry

The results of this procedure, for each sample, can be seen below:

**Power variation samples**

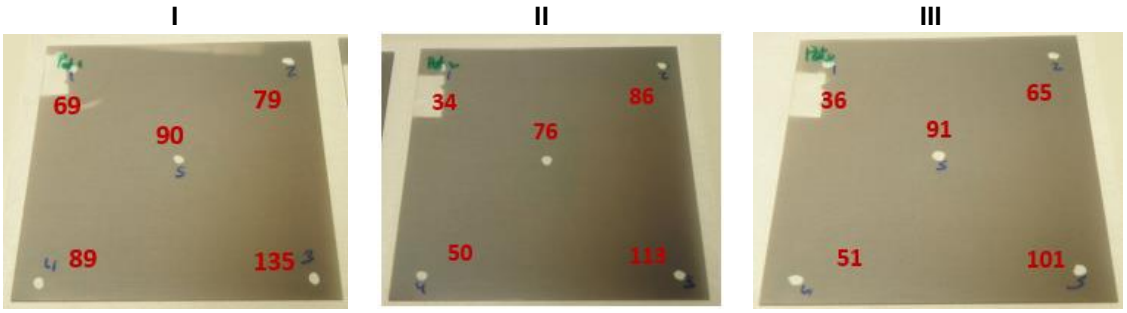


Figure 4.5 - Thickness results [nm]: samples I (100W 40min), II (125W 30 min) & III (150W 20min).

From the profilometry results (Fig 4.5), it can be seen that sample I has the thickest thin film layer, whilst sample III has the slimmest. This may be due to time exposure during deposition. However, to get the growth rate of the thin film that was deposited per minute, we divided the point with the highest value [nm] (point 3) by the total deposition time.

Table 4.6 - Sample I, II & III growth rate

| Sample | Growth rate (nm/min) |
|---|---|
| I | 3,38 |
| II | 3,77 |
| III | 5,05 |

The rate values in table 4.6 indicate that sample III has the highest rate. This means that, although it had the shortest deposition in time, there were more atoms deposited per minute, in

comparison with the other samples. This indicates that, with more power applied in the process, there were more atoms released from the target, hence the highest ratio in sample III.

**Deposition pressure samples**

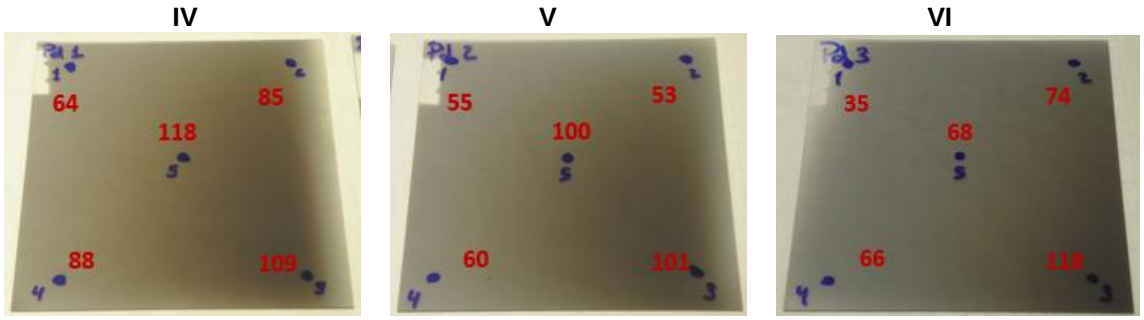


**Figure 4.6 - Thickness results [nm]: samples IV (6.0E-3 mbar at 30 min), V (8.0E-3 mbar at 30 min) & VI (1.0E-2 mbar at 30 min).**

The results obtained (Fig. 4.6) show less thickness differences between the three samples. Contrary to the previous samples, point 3 was not properly covered by particles, due to shutter misplacement. Therefore, we chose point 5 to compare the samples' thin film growth ratio. The results are shown in table 4.7:

**Table 4.7 - Sample IV, V & VI growth rate**

| Sample | Growth rate (nm/min) |
|---|---|
| IV | 3,93 |
| V | 3,33 |
| VI | 2,27 |

The ratio results show that with the pressure increase during depositions, particle deposition has decreased. From sample IV to VI, there was a ratio reduction of nearly 58%.

**$O_2$ Flow**

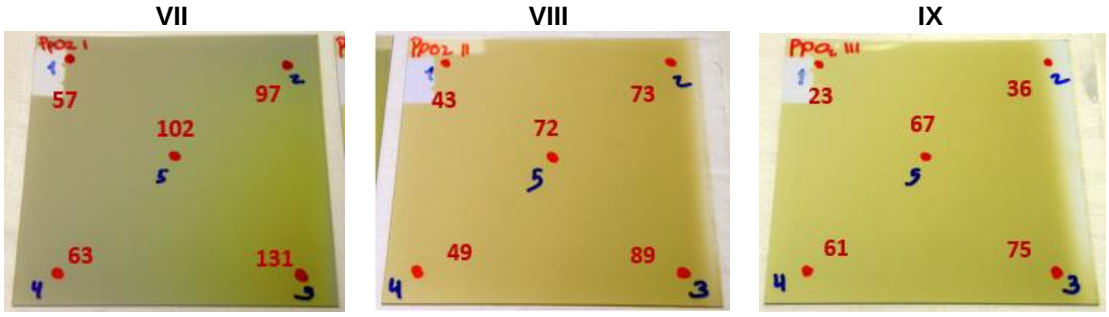


**Figure 4.7 - Thickness results [nm]: samples VII (1 sccm 30 min), VIII (2.5 sccm 30 min) & IX (5 sccm 30 min).**

Results show (Fig. 4.7) that there has been a reduction in thickness, from sample VII to IX. This might be due to reactions between the target's released particles and the reactive gas ($O_2$) introduced in the process. The point chosen for ratio comparison was point 3, which presents good film coverage in each sample. The ratios can be seen in table 4.8:

Table 4.8 - Samples VII, VIII & IX growth rate

| Sample | Growth rate (nm/min) |
|---|---|
| VII | 4,37 |
| VIII | 2,97 |
| IX | 2,50 |

The ratios indicate that, with more $O_2$ flow introduced in the process, the thickness of the films have also decreased. This effect occurs is explained by the increased pressure values that contribute to higher oxidation of $VO_2$ particles. From sample VII to IX there was a decrease of nearly 57%.

### 4.2.2 Morphological and structural characterization

After obtaining all the thin films samples on the glass plates, they were cut into smaller pieces (Fig. 4.8) for the XRD analysis.

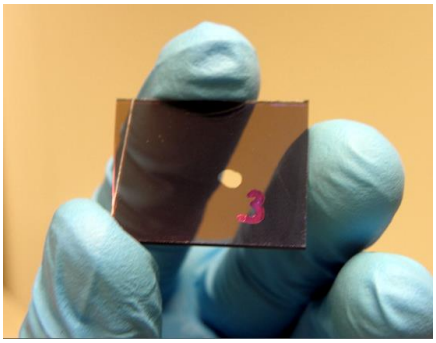


Figure 4.8 – Sample cut example.

#### Annealing

The annealing of all samples was made at a temperature of 450 ºC, during 2 hours. The inert gas used during the process was nitrogen (N). The temperature chosen was based on other studies about thermochromic $VO_2$ [21][31].

#### X-Ray diffraction

After annealing, the samples were taken to XRD analysis. The main purpose was to identify whether the thin films were in $VO_2$ state, or another VOx phase.

The analysis showed that most of the samples' structures were amorphous, with exception for those in which the $O_2$ flow was controlled (VII, VIII & IX). In these, the $VO_2$ phase was not identified. The X-Ray data can be seen in Annex. The cause for the absence of this phase on all samples might be due to the fact that bare glass is not resistant to such a high temperature (450 ºC), and has released particles that affected the optical properties of the films. It is also likely that the heat might have irreparably damage the glass morphologic structure, especially the surface in contact with the film, affecting the film, also.

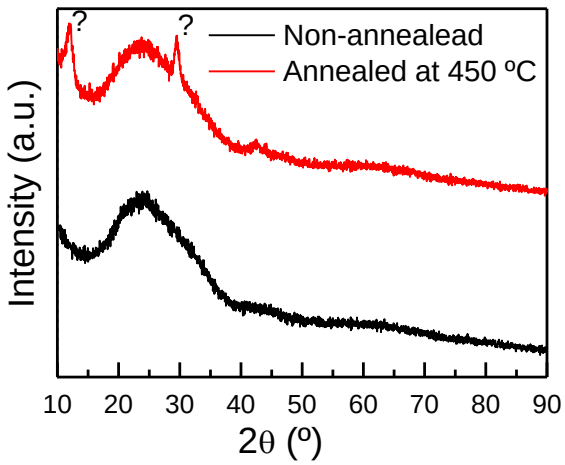


**Figure 4.9 - XRD patterns obtained from $VO_2$ deposited on glass, with $O_2$ flow of 1 sccm.**

### 4.2.3 Anomalies, causes and corrections

The first results were not as initially expected, with the samples' structures being amorphous, mostly. Moreover, the spectroscopy tests revealed that the samples didn't show any relevant thermochromic behavior when exposed to a temperature gap from room temperature (RT) to 100 ºC. As referred previously, bulk-like $VO_2$ is expected to change its behavior at approximately 68ºC [34], which didn't occur during these tests.

The causes for this were not certain. Probable causes could be the fact that the substrate (glass) wasn't suitable to handle the annealing temperature (450 ºC) for the referred time period (2H) and interfered with the samples' crystalline formation. Another possible cause could be the formation of a different VOx phase, during the deposition process. A less likely factor could have been a system malfunction or anomaly in the equipment utilized. As a consequence, it was decided to repeat the depositions, paying attention to the following factors:

- Change the glass substrate to another more resistant to heat, such as $Al_2O_3$ or Corning glass.
- Double-check the equipment conditions before and during the process/analysis
- Make further annealing tests, at 450 ºC, 550 ºC, 650 ºC and 750 ºC for 2H, each.

Furthermore, Montero *et al* and *R. Marvel et al* studied how different types of substrates could affect the thin films' crystalline structure. It was concluded that depositions on bare glass formed a poor crystalline structure. As a consequence, it would show a lower conductive behavior [35], [36]. Other studies indicate that prolonged annealing time (4H-7H) can lead to better growth orientation and larger grain sizes in $VO_2$ films [37], [38].

New depositions were made using $Al_2O_3$ substrates, in two different conditions. One would be absent of $O_2$, and the other would have a minimum $O_2$ flow. We calculated the approximate deposition time based on the first profilometer results. The new conditions are shown in Table 4.9.

**Table 4.9 - New deposition conditions on $Al_2O_3$ substrate**

| P (W) | T (min) | Pdep (mbar) | Ar (sccm) | $O_2$ (sccm) | DC Bias (V) | Pump speed (rpm) |
|---|---|---|---|---|---|---|
| 125 | 80 | $4.0x10^{-3}$ | 37 | 0 | -180 | 21600 |
| 125 | 60 | $4.0x10^{-3}$ | 36 | 1 | -200 | 21600 |

With the depositions complete, both samples were cut into smaller rectangular pieces, to anneal at different temperature conditions.

### 4.2.4 Optical properties

After annealing the new samples, there were made spectroscopy tests. All the samples were first analyzed at room temperature (RT) and then at 100 ºC. The results obtained from the Ar-$O_2$ sample didn't show any change in reflectance. This may be due to the possibility of having a different VOx phase, and as a consequence, the $T_c$ is higher than 100 ºC. Besides the yellowish color of the films obtained, which can be seen as an oxidation sign, XRD analysis did not indicate the presence of $VO_2$. On the other hand, the oxygen-free sample showed presence of $VO_2$, from XRD. Moreover, we obtained relevant results of its thermochromic behavior when exposed to a temperature range from room temperature to 100 ºC. The results are shown below:

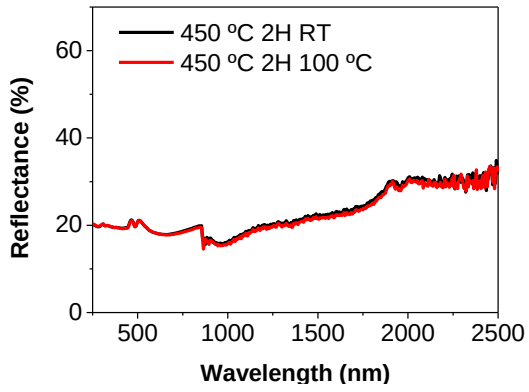


Figure 4.10 - 2H annealing at 450 ºC

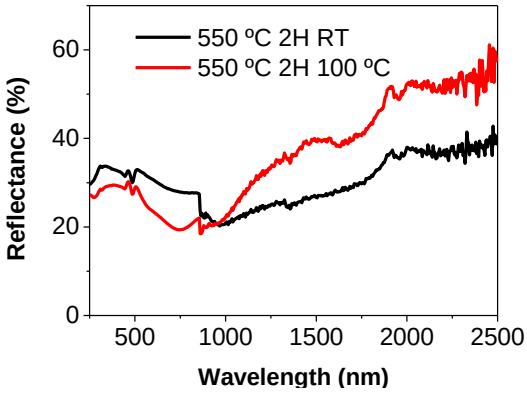


Figure 4.11 - 2H annealing at 550 ºC

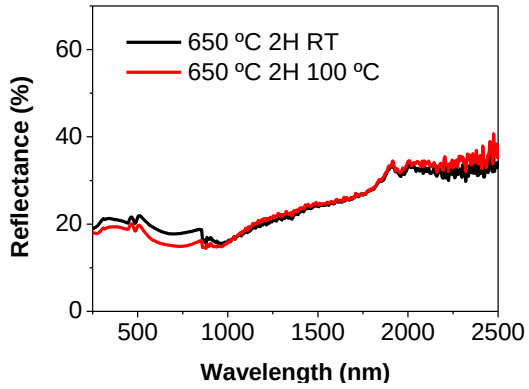


Figure 4.12 - 2H annealing at 650 ºC

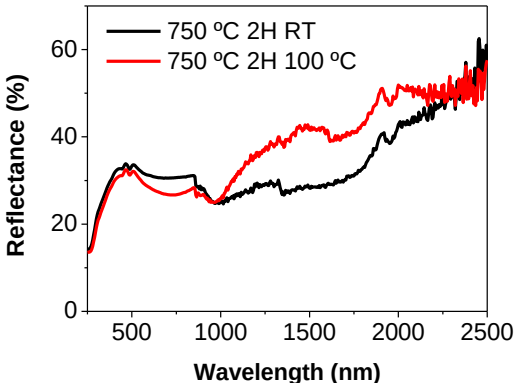


Figure 4.13 - 2H annealing at 750 ºC

Comparing the results, it was clear that the most interesting was the sample annealed at 550 ºC (Fig. 4.11). Between the 2000 nm to 2500 nm range, the reflectance difference reaches nearly 20%. From 2000 nm to 900 nm, the difference gradually decreases until it reaches zero. In the visible zone, the difference is inverted to nearly 10%. From 500 nm to 250 nm, it showed a minor reduction, however, it never reached zero.

Looking at a construction glazing perspective, where we want NIR to be blocked and VR to pass through the film, this result showed an interesting outcome. Furthermore, we also analyzed two samples with lower annealing times. The annealing was made at 550 ºC, for 1H and 30 min. The results were not so interesting, therefore we kept the optimal parameters (2H at 550 ºC) for the following depositions. The charts of the two samples can be seen in Annex A.

For the next set of depositions, Corning glass was used, instead. This type of glass resists to higher temperatures than normal glass and is the closest simulation to a "smart" window than $Al_2O_3$ substrate. The deposition parameters were the same as the previous.

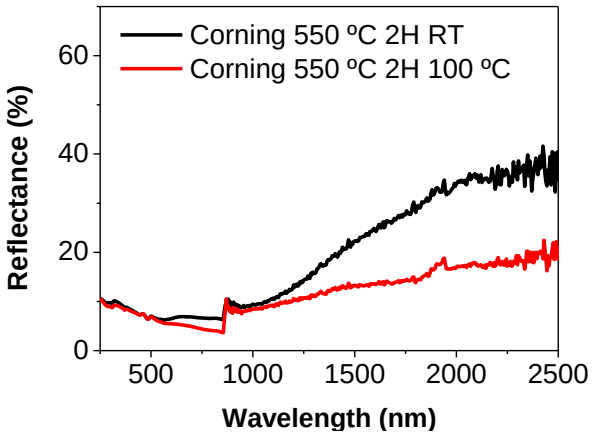


**Figure 4.14 - Corning glass substrate annealed for 2H at 550 ºC**

The results showed a very different behavior of the sample when analyzed with the spectrophotometer (Fig. 4.14). Contrary to the previous set of depositions on $Al_2O_3$ substrates, which showed higher NIR reflection above the critical temperature (± 68 ºC), this sample showed an opposite effect.

When exposed to 100 ºC, the sample's reflectance in the NIR zone appears lower than at room temperature. Theoretically speaking, this means that a window coated with the exact same material, when exposed to a temperature higher than the $T_c$, instead of reflecting more IR radiation, would let it pass more easily. For this reason, it would be unsuitable for buildings as it would affect greatly their interior temperature, rising it more when it was already high.

In the NIR zone, it can have a difference range of nearly 20%. On the other hand, in the visible zone shows little difference, but still lower than the room temperature's result. The real cause for this effect to occur was not certain. However, there could be a probability of anomaly during the sputtering and/or annealing processes.

To help uncovering the cause, we repeated the annealing process with non-annealed samples from the same deposition set at 450 ºC for 30 min and 550 ºC 30 min. Both samples showed similar effect after the spectrophotometer testing. This indicated that the problem was not related to the annealing process. These results can be found in the Annex A.

Furthermore, a new deposition was made and annealed at 450 ªC and 550 ºC, with different times. The correspondent graphs can be found in Annex A. Table 4.10 represents the results, after spectroscopy analysis:

**Table 4.10 - Results after spectroscopy analysis**

| Annealing temperature | Substrate | Time (min) | Effect >$T_c$ |
|---|---|---|---|
| n.a | Corn. | 0* | None |
| 450 | Corn. | 30 | Lower IR reflectance |
| 550 | Corn. | 30 | Lower IR reflectance |
| 550 | Corn. | 120 | Lower IR reflectance |

**non-annealed sample*

The spectroscopy tests inevitably showed the same effect as the previous deposition, with Corning glass. At this phase, the cause for these unpredictable measurements remained uncertain. However, it is likely that the spectrophotometer equipment is not suitable for glass analysis of this type.

Complementary SEM analysis were made to the previous samples, to observe their surface structure (Fig. 4.15). After annealing, it is possible to observe crystal formations on the samples. Additional SEM images can be seen in Annex B.

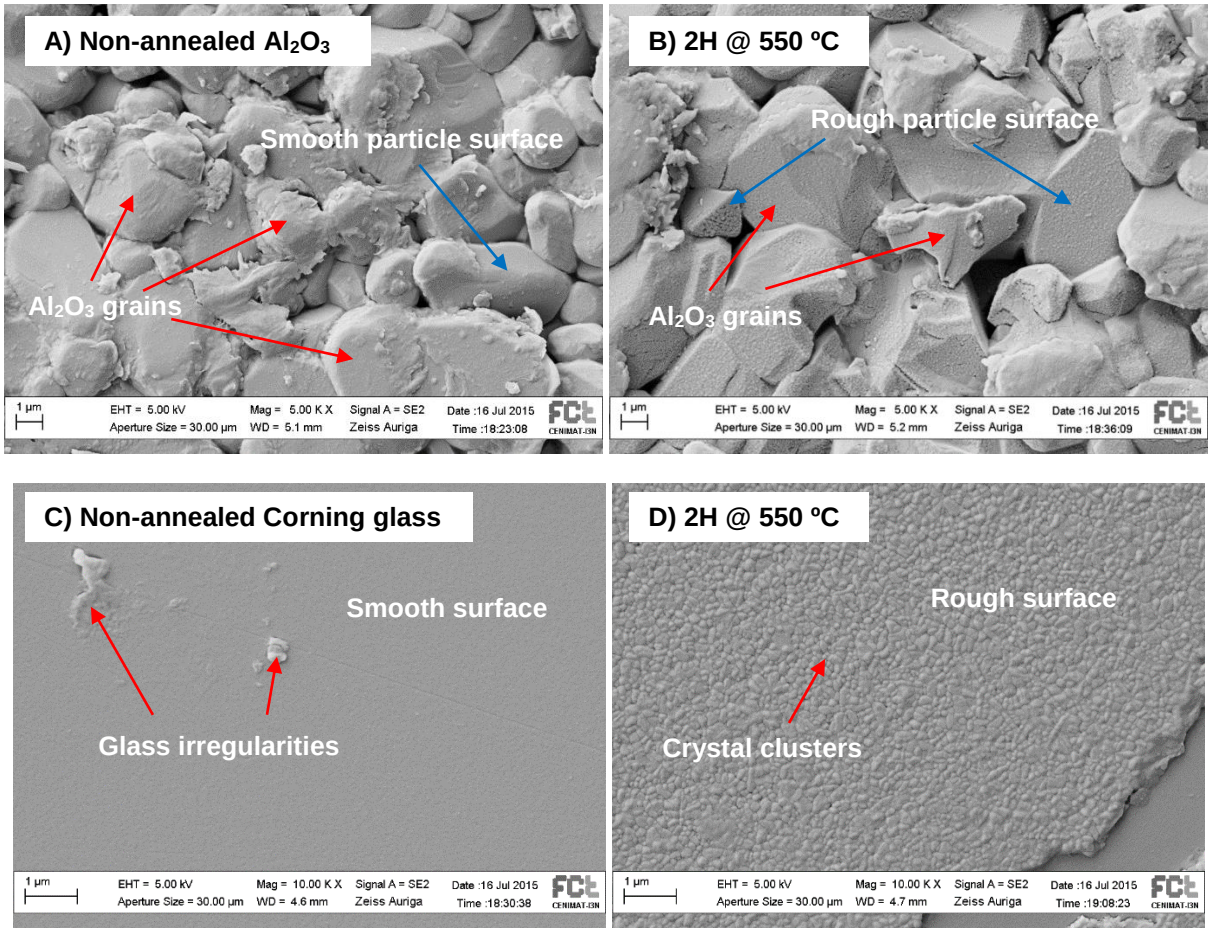


**Figure 4.15 – SEM images of $VO_2$ films deposited on $Al_2O_3$ and Corning glass samples, before (A,C) and after (B,D) annealing.**

The images above show crystalline formations, in both substrates, $Al_2O_3$ and Corning glass (Fig 4.15, A and B respectively). The rough surface of each substrate, after annealing, is due to the formation of crystal clusters, possibly of $VO_2$, as it was expected.

### 4.2.5 Thin films doping via co-sputtering

In the co-sputtering process, it was relatively complex to determine the optimal parameters for the depositions. Since there were two different targets, a 2 inch $VO_2$ target and a 3 inch $WO_3$ target, it was considered that it should be a try-and-error procedure until the results reach an optimal state.

Both targets were 10 cm away vertically from the substrate. However, due to the machine's configuration, one of the targets ($VO_2$) was positioned at an angle (+/- 60º). During the deposition, the substrate rotated at 15 rpm, to ensure better homogeneity of the films. After several attempts to optimize the co-sputtering conditions, the most significant results were obtained with the conditions found in table 4.11.

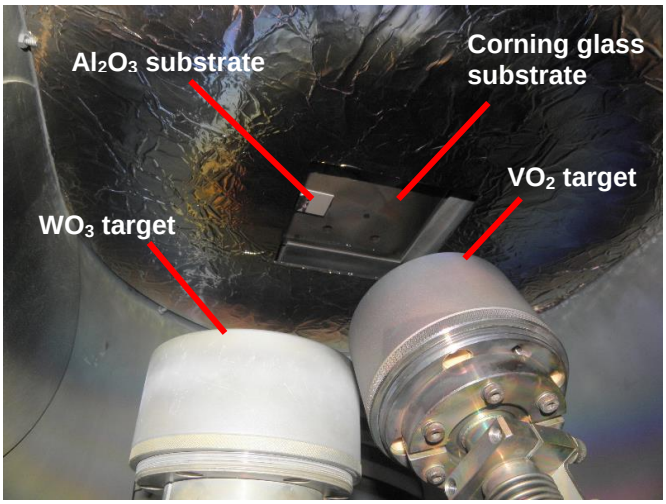


**Figure 4.16 - Vacuum chamber before co-sputtering.**

**Table 4.11 - Co-sputtering conditions.**

| Target | P (W) | T (min) | Pdep (mbar) | Ar (sccm) | $O_2$ (sccm) | DC Bias (V) | Pump speed (rpm) |
|---|---|---|---|---|---|---|---|
| $VO_2$ | 125 | 30 | $4.0x10^{-3}$ | 33 | 0 | -287 | 21600 |
| $WO_3$ | 10 | | | | | -95 | |

The conditions above (table 4.11) were determined after several co-sputtering depositions, followed by annealing and spectroscopy analysis, to observe the behavior of each doped thin film. With the deposition conditions optimized, a final deposition was made, in order to draw the most significant data from its optical properties. After the last deposition, the sample was cut into smaller pieces, which were annealed at different temperatures and times. After annealing, spectroscopy analysis were made to observe if the doped films were behaving as expected, by having higher NIR reflectance with a $T_c$ lower to the bulk-like form ($T_c$ < 68 ºC).

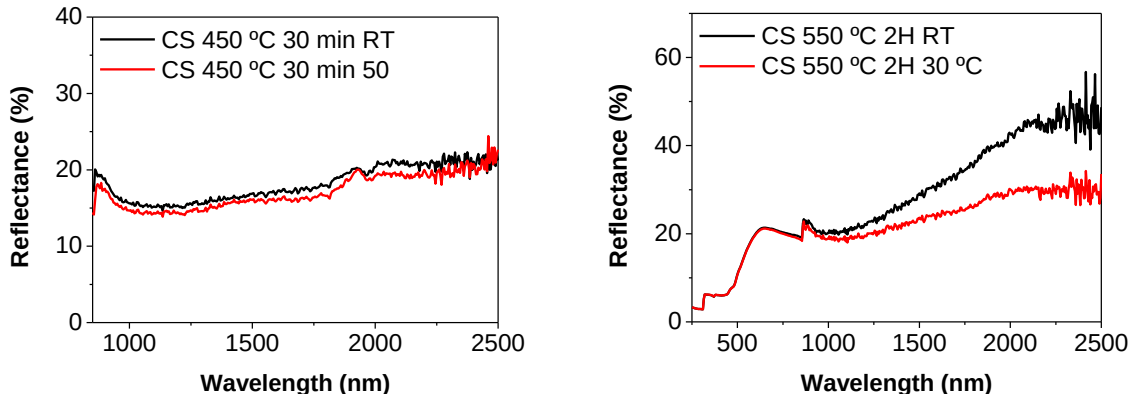


**Figure 4.17 - Sample annealed at 550º C, 2H; Sample annealed at 450º C, 30 min.**

In the graphs above (Fig. 4.17), it can be seen that the first attempt of co-doping $VO_2$ thin films with $WO_3$, proved successful. As expected, both samples showed phase transition (semi-conducting – metallic) at lower temperatures than in bulk-like form (<68 ºC). However, the reflectance was expected to increase with temperatures above RT, which did not happen. The likely cause for this effect was mentioned previously, concerning the spectroscopy analysis inappropriate for glass testing.

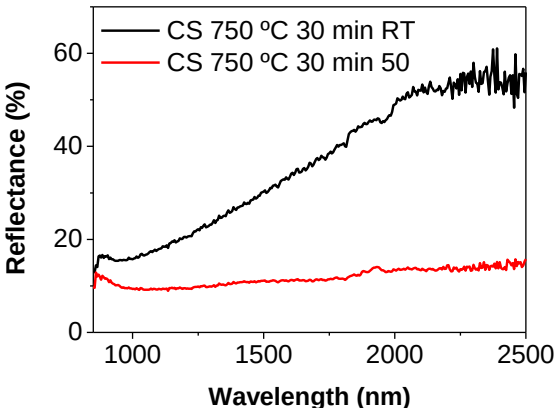


**Figure 4.18 - Sample annealed at 750 ºC, 30 min.**

An additional annealing procedure was made, with higher temperature than the previous samples, followed by spectroscopy analysis (Fig. 4.18). The results showed a similar effect as the previous samples, with the reflectance decreasing with temperatures above RT. However, in the IR zone from 2000 nm to 2500 nm, there was a major decrease of nearly 40%. Comparing with the previous results, it can be seen that, with higher annealing temperature, a greater reflectance gap is observed. This may be due to a higher crystal formation in the co-doped films, which could lead to their better conductivity. Y. Guo *et al* concluded in a recent study that prolonged annealing time of VO2 thin films can lead to better growth orientation, larger grain size and good phase transition properties [37]. Nonetheless, using RF magnetron sputtering to create efficient smart windows proved to be unsuccessful, as the effect obtained on glass substrates was always the opposite as predicted initially.

## 4.3 Smart tiles

### 4.3.1 $VO_2$ nanoparticles production

The ST is basically a regular ceramic tile, coated with a thermochromic set of layers. The process of application of the coating is defined by four main phases: solution production, drying, spray-coating and annealing.

**Production of $VO_2$ nanoparticles by hydrothermal synthesis**

A $VO_2$ pre-solution was obtained by mixing in water $V_2O_5$ (Sigma Aldrich, 98%) with $C_2H_2O_4 \cdot 2H_2O$ (Merck) and doped with 3% $WO_3$ (Aldrich). The solution was mixed during 20 minutes to ensure a complete homogeneity of the solution (Fig. 4.19).

**Figure 4.19 - $VO_2$ pre-solution mixing.**

### Microwave irradiation and drying

After the mixing, the solution was taken into the microwave (CEM, Discover) for 40 minutes, giving a final $VO_2$ solution (Fig. 4.20). Afterwards, it passed through centrifugation to remove the majority of the water. To completely dry out the powder, it was left on a heat plate, in a vacuum chamber, overnight. Finally, the different sized grains were grinded to obtain a homogenous $VO_2$ powder.

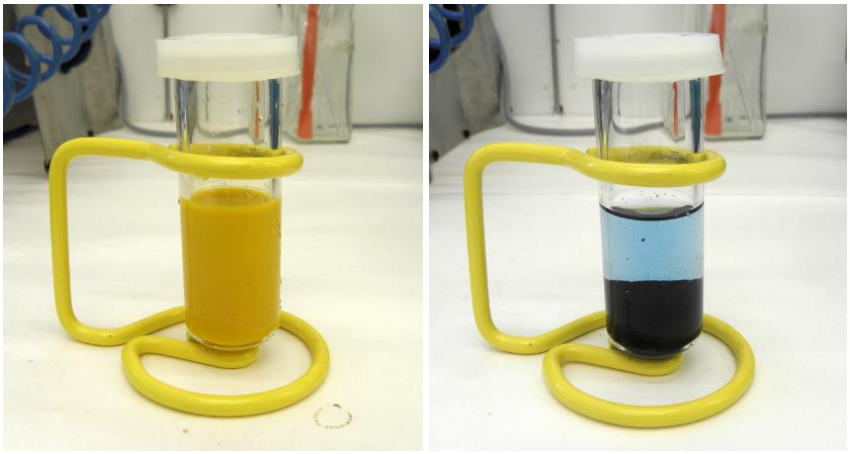

**Figure 4.20 - $VO_2$ solution (right) after the microwave process.**

### Spray-coating phase

To apply the powder onto the tiles' surface, we used a $CO_2$ spray canister. The canister was filled with water and added the $VO_2$ powder on a 10 mg/ml concentration. To ensure immediate adherence of the particles, the tiles were heated at 120 ºC using a hoven (TK 4067, Ehret). When the solution was sprayed onto the surface of a tile, the water vaporized, leaving only the $VO_2$ particles. The average $VO_2$ quantity used was 0.016 g/cm2.

**Figure 4.21 - Smart tile and regular tile comparison.**

When compared with a regular tile, the ST presents a dark grey color, and rough surface (Fig. 4.21). The non-annealed coating presents poor adherence to the ceramic tile, capable of being partially eroded by simple passing a finger over the coating. After annealing, the coating adherence proved to be much stronger, resisting to finger rubbing.

### Annealing

The tile fragments (2.5 cm x 2.5 cm) tested in laboratory, were annealed during 2H, at 750 ºC in the tube furnace, with Ar. The temperature set was required for better particle adhesion.

Due to the size of each tile, special equipment was needed for annealing. All the tiles were annealed during 2H, at 750 ºC in vacuum, in an industrial furnace, property of CTCV – *Centro Tecnológico da Cerâmica e do Vidro*, in Coimbra.

### 4.3.2 Structural and optical properties

Smaller samples were analyzed by optical microscope and spectrophotometer. They showed the expected behavior when submitted to temperature changes, by increasing their reflectance in the NIR. Unexpectedly, the tiles showed increasing levels of layer erosion and oxidation, over time. Moreover, microscopy analysis was made before and after the tiles were exposed do daylight, during one month (August). The results showed a significant decrease in the layers on many tiles and also signs of oxidation (Fig. 4.23). Additional images can be seen in Annex D.

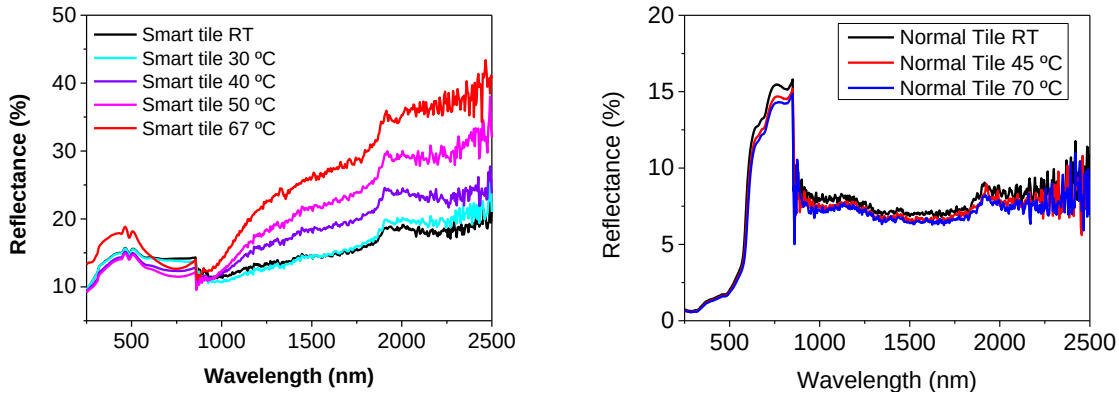


**Figure 4.22 - Smart tile and normal tile reflectance testing before exposure to real atmospheric conditions.**

Fig. 4.22 represents the results of a "new" ST sample spectroscopy analysis with different temperatures, in comparison with a normal tile. It can be seen that the tile coating, doped with 3% $WO_3$ has successfully reduced the $T_c$ from 68 ºC to nearly 30 ºC. The results of two ST samples were also compared, to observe the coating's performance after one month exposed to RAC (Fig. 4.23).

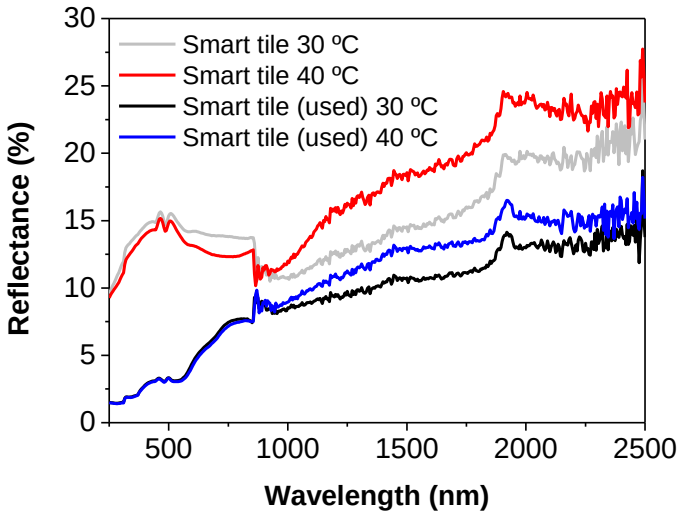


**Figure 4.23 - Optical performance comparison between a new and a used smart tile.**

Fig. 4.23 shows a graphical comparison between the ST coating before and after (used) being exposed to RAC, during one month. It clearly shows a significant loss in reflectance in the IR zone (up to 25%), for different temperatures. Vis and UV radiation reflectance is also greatly decreased. The performance loss was caused by layer erosion over time and partial oxidation of the coating.

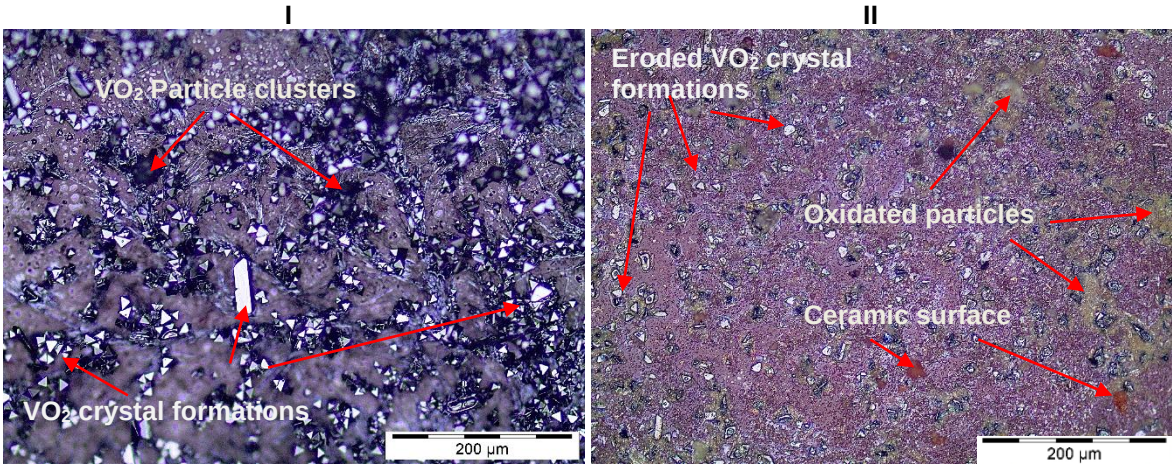


**Figure 4.24 - Tile surface - I) immediately after annealing II) after one month of exposure to real atmospheric conditions.**

The images above show a microscopic comparison of a ST coating before and after exposure to RAC. While the image on the left (I) presents full coverage of the tile's surface, the image on the right (II) shows clear signs of layer erosion, oxidation and visible ceramic surface, which has affected ST's performance over time.

## 4.4 Smart paints

The smart paints study was made in collaboration with CENIMAT's staff, during the same time period of this work. The idea was simple: mix $VO_2$ doped powder with an exterior white paint and study its optical properties. In the possibility of having positive results, the smart paint would be applied to the house models of this work, studying its effect in RAC, alongside the glass and the tiles.

The production of $VO_2$ powder for the paint was identical to the tiles – hydrothermal synthesis with microwave. The powder was mixed in different concentrations and its optical properties tested multiple times on $Al_2O_3$ plates (Fig. 4.25). While the coating on the tiles produced positive reflectance results, the same effect in the paint was inexistent. The most likely cause for it, was the high number of chemicals in the original paint that could have reacted with $VO_2$, changing its properties. However, the finding of the real cause would represent a comprehensive and time consuming study. For that reason, its inclusion and application in this work was left aside.

**Figure 4.25 - Smart paint application on $Al_2O_3$ plates.**

The image above (Fig. 4.25) shows multiple Al2O3 plates painted with different concentrations of $VO_2$ | $WO_3$ powder. None of the samples tested showed positive optical results. The application of "smart" paints was unsuccessful.

## 4.5 House model

In this sub-chapter, it will be shown the design, creation and testing of two structurally identical house models, in real conditions of solar irradiance. The purpose was to apply windows and ceramic tiles with TC coatings, such as thin films and paints, respectively, to one of the models. Next, we would measure the interior temperature data of both models and compare them. In theory, the model equipped with thermochromic materials would present a lower interior temperature during the day, compared with the thermochromic-free model.

### 4.5.1 Project

The house model should be both inexpensive and similar to a real wooden house. In Portugal, the most used material in the construction sector for housing is concrete. However, we chose wood to lower material costs and make it easier to build. Moreover, wood is lighter and more versatile than concrete, making it easier to transport anywhere. The roof would be coated with miniature ceramic tiles. In addition, a single window would be made in in the façade facing south. This way, it would be optimized to receive the most sunlight, especially during the hottest periods of the day.

With that in mind, the first architecture design was made on paper (Fig. 4.26). The measurements where defined, as well as the construction materials needed for building both models. Secondly, based on the previous sketch, a digital 2D model was designed, using the software program *AutoCAD*®.

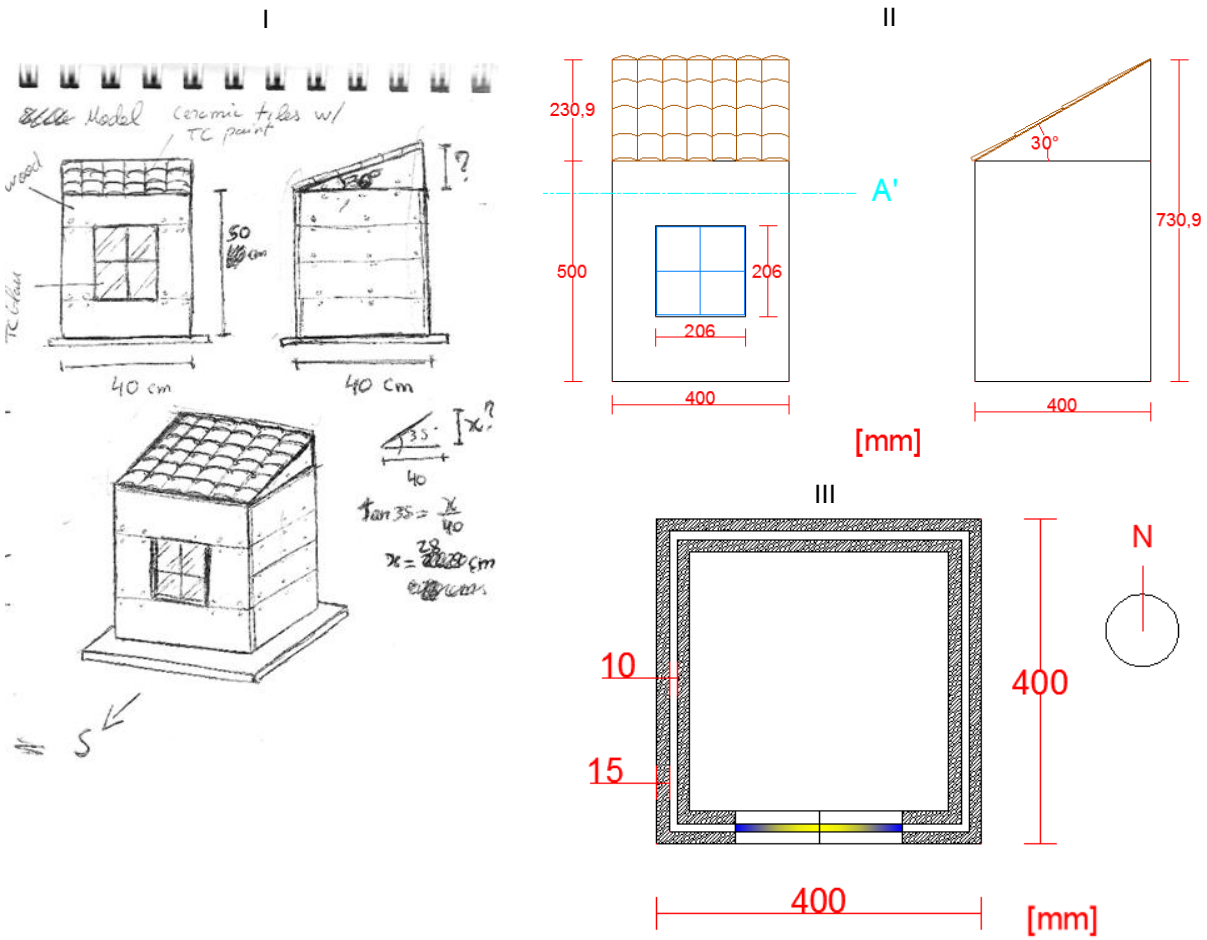


**Figure 4.26 – First house model draft (I); North and east facades (II); Model plan (III).**

The next step was to give the design a 3D shape (Fig. 4.27). In order to do this, it was used the software program *SketchUp® Make*.

Figure 4.27 - 3D concept

**Materials**

The main material used for construction was OSB (Oriented Strand Board). Due to its fabrication process, this product offers many advantages when comparing to standard plywood [39]. The most important are listed below:

- High mechanical resistance
- Resistance to deformation
- Great relation resistance to weight
- High durability in humid climates
- Easy to use: OSB can be easily cut, drilled and sanded.

Figure 4.28 - OSB wood planks.

Moreover, in order to fix the planks to each other it was used glue, reinforced with standard screws and aluminum plates for additional mechanical resistance.

### 4.5.2 Construction procedures

The construction procedures took place at CEMOP's workshop. Firstly, it was important to have planks with exact measures. Professional help was necessary for this step (**1**). Secondly, all pieces were numbered to ease the construction process, avoiding mounting mistakes. Afterwards, guidelines of the walls were marked, on each base, giving a previous look of the next step (**2**). As the bases were prepared, we added aluminum joints to support the interior walls, while adding increased mechanical resistance (**3**). The joints were made manually, cutting smaller pieces out of a large plank and making the holes with a driller.

**1** **2**

Figure 4.29 - 1) OSB wood planks for the models; 2) Base detail.

In order to ensure the exterior walls would have the same resistance to exterior forces as the interior walls, they were attached together using long screws, combined with washers and screw-nuts for spacing and fixing (**4**).

**3** **4**

The next step was to mount all the walls, fixing them to each other (**5**). In the process, the sidewalls were cut according to the respective roof angle (30º). Additional aluminum joints were installed in the corners of the walls. After all walls were connected, the roof structure was built to hold 24 tiles, each. Single front-wall window holes were made for the possibility to add functional smart windows in a future work (**6**). Finally, three temperature sensors were installed in each model. One sensor outside, and two inside: one in the middle of the house and another directly beneath a center roof-tile. This way, the outside and interior temperatures would be registered, alongside the temperature of the tile.

The models were moved to CEMOP's rooftop, with the front walls facing south, for optimal irradiation exposure (Fig. 4.30). The data collection was made during August.

**5** **6**

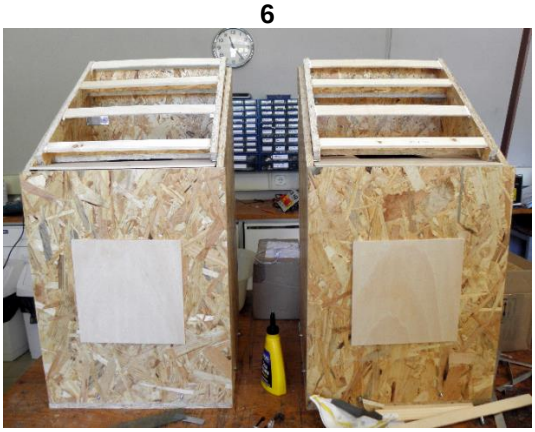

**Figure 4.30 - House models in the testing site. The roof on the left has regular tiles, while the roof on the right has "smart" tiles.**

In the previous image, it can be observed the final look of the house models, on the roof of CEMOP. Both were equipped with temperature sensors. The house on the right had installed “smat” tiles, while the house on the left had regular tiles.

### 4.5.3 Sensors data

The data gathered from the sensors in the models, revealed contrary evidence of what was initially expected (Fig. 4.31). It was expected that the interior temperature of the house with the ST tiles on the roof would present a lower interior temperature, which didn’t occur. After testing and observing the ST’ optical properties, it was predicted that the roof coated with $VO_2$ layers would prevent higher temperatures inside, when compared to the model without any coating. The results show that the temperature of the smart tiles was always higher than the normal tiles. Consequently, the temperature inside the correspondent model was also higher, especially during peak hours (12H-16H).

A possible reason for the higher temperature increase in the smart tiles is the fact that, by presenting a darker color, it can lead to greater heat absorption. As a consequence, heat is radiated to the interior of the model, thus increasing its temperature. The basic model insulation might also have contributed to high heat gains inside, which is also favored in case the coating is active.

The sharp temperature variations during the day, especially in the tiles, may have been likely caused by external atmospheric elements, like the wind and passing clouds, thereby preventing full irradiation exposure, lowering the surface temperature.

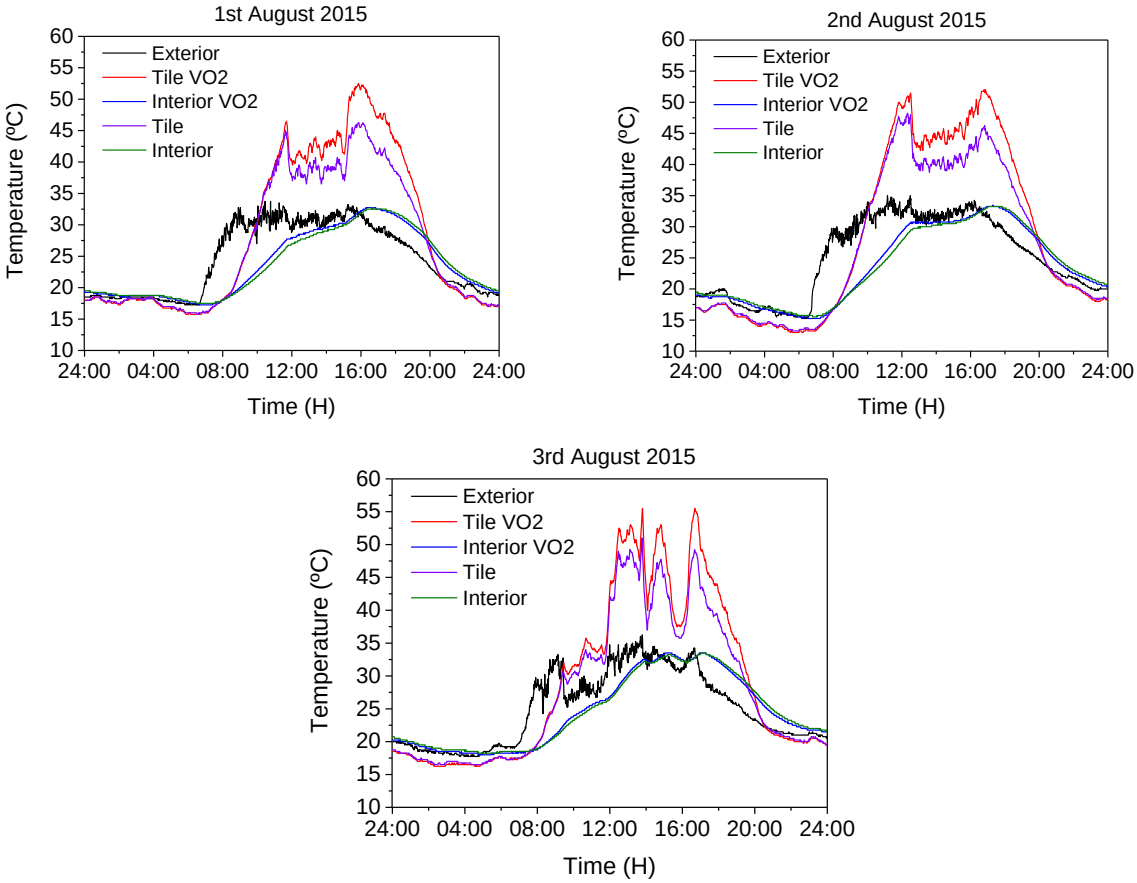


**Figure 4.31 - Sensor data of both models, in real conditions.**

The effect observed is far from what was expected. Nonetheless, the testing of the $VO_2$ coatings on a roof with real ceramic tiles was successful.

# 5. Conclusions and future work perspectives

The aim of this work was to study and test one of the most studied thermochromic materials – $VO_2$. Thorough research was undertaken in order to comprehend and explore its unique optical properties, one of which with great interest – its higher reflectance properties in the NIR zone with temperature increase. One of the main efforts was to include $VO_2$ in different architectural elements on scaled models, studying and comparing the house models interior temperature, in real atmospheric conditions.

## 5.1 Conclusions

Through this work, it was possible to apply $VO_2$ in three different construction materials – glass, ceramic roof-tile and paint – using two approaches: physical and chemical methods. The construction of two identical house models was made in order to properly test the combined effect of these elements, when exposed to real conditions. Glass and paint application proved unsuccessful, due to their poor results in laboratory, showing an opposite optical effect - reflectance decrease with temperature - or none at all. In the case of glass, thin films were produced by RF magnetron sputtering, varying different parameters and conditions. Normal glass proved unsuitable for high annealing temperatures, from 450 ºC, to 750 ºC. Corning glass and $Al_2O_3$ substrates were tested, instead. While the latter showed positive optical results (15% to 18% reflectance increase in 1200 nm-2000 nm), the results obtained with Corning glass were unsatisfactory for smart windows application (18 % to 20 % reflectance decrease in the same range).

Similar effect occurred with the co-sputtered samples of $VO_2$ and $WO_3$. One of these showed a significant decrease in reflectance of nearly 70% (1200 nm – 2000 nm). The real cause for the opposite effect was not determined. However, the characterization method for glass samples could not be the most appropriate, which might have led to believe the inefficiency of the thin films obtained by sputtering.

$VO_2$ application onto ceramic tiles through hydrothermal synthesis with microwave and spray-coating showed positive optical results in laboratory, though. Optical tests showed nearly 20% increase in reflectance, for the wavelength range of 1200 nm-2000 nm. After this point, the focus of this work shifted to the smart tiles application in the house models.

The final data gathered from the models showed that the roof coated with $VO_2$ layers contributed to higher heat gains, in the correspondent model. Deficient insulation and poor thermochromic efficiency may have contributed for this increase. Moreover, after one month exposed to real atmospheric conditions, most of the smart tiles showed signs of layer erosion and oxidation, which led to performance loss of the coating, over time. Later microscopic observations confirmed the erosion of most of the crystalline structure of the tiles' surface and partially oxidized areas. It is important to mention that the tiles installed in the house models were annealed in vacuum, while the annealing of laboratory samples used Ar, as the inert gas.

Thermochromic coatings are still far from great, however, they can lead to interesting new ways of passive energy-saving techniques. Nevertheless, various improvements are to be made in order to obtain better results of the coatings.

## 5.2 Future work perspectives

One of the most interesting points to study in a future work, is how to improve the effectiveness of $VO_2$ thin films on glass substrate. The discovery of the reason behind the opposite optical effects obtained using glass substrates is necessary. Analyzing the samples with an appropriate method for glass optical testing should lead to real reflectance results. Different deposition processes and substrates can lead to other interesting results [36]. With positive results for smart windows application, it would represent an interesting area of research. Furthermore, both house models were prepared to have windows installed in the front wall, opening way to test their efficiency in RAC.

Another point to be assessed in a future work, would be how to improve smart tiles thermochromic performance and durability, using $VO_2$ layers. A research to lower the transition temperature of VO2 is also recommended, since it would improve the tiles' efficiency in reflecting NIR radiation at average temperatures (25ºC – 28 ªC), during the summer. The house models can be used to test the tiles, also. However, their insulation improvement would also be strongly recommended in order to have the least thermal transfers possible. Using efficient materials like extruded polystyrene (XPS) or mineral wool, would reduce heat gains by presenting low conductivity coefficients.

# 6. Bibliography and references

In this chapter is included the bibliography and all the references made in this work.


[1] L. Pérez-Lombard, J. Ortiz, and C. Pout, “A review on buildings energy consumption information,” *Energy Build.*, vol. 40, no. 3, pp. 394–398, 2008.

[2] J. Morrissey, T. Moore, and R. E. Horne, “Affordable passive solar design in a temperate climate: An experiment in residential building orientation,” *Renew. Energy*, vol. 36, no. 2, pp. 568–577, 2011.

[3] H.-Y. Chan, S. B. Riffat, and J. Zhu, “Review of passive solar heating and cooling technologies,” *Renew. Sustain. Energy Rev.*, vol. 14, no. 2, pp. 781–789, 2010.

[4] R. V. Ralegaonkar and R. Gupta, “Review of intelligent building construction: A passive solar architecture approach,” *Renew. Sustain. Energy Rev.*, vol. 14, no. 8, pp. 2238–2242, 2010.

[5] B. Su, “The impact of passive design factors on house energy efficiency,” *Archit. Sci. Rev.*, vol. 54, no. 4, pp. 270–276, 2011.

[6] J. Fernandes, R. Mateus, L. Bragança, and J. J. Correia da Silva, “Portuguese vernacular architecture: the contribution of vernacular materials and design approaches for sustainable construction,” *Archit. Sci. Rev.*, vol. 58, no. 4, pp. 324–336, 2015.

[7] “Trombe Wall,” 2008. [Online]. Available: https://upload.wikimedia.org/wikipedia/commons/3/3d/Illust_passive_solar_d2_319pxW.gif. [Accessed: 03-Sep-2015].

[8] M. Fordham, “Natural ventilation,” *Renewable Energy*, 2000. [Online]. Available: https://upload.wikimedia.org/wikipedia/commons/thumb/5/58/Malqaf.jpg/1280px-Malqaf.jpg. [Accessed: 03-Sep-2015].

[9] R. Estate, “Green Roofs,” 2013. [Online]. Available: https://c2.staticflickr.com/4/3482/3926468274_1185491b6b_b.jpg. [Accessed: 03-Sep-2015].

[10] C. G. Granqvist, S. Green, G. A. Niklasson, N. R. Mlyuka, S. von Kræmer, and P. Georén, “Advances in chromogenic materials and devices,” *Thin Solid Films*, vol. 518, no. 11, pp. 3046–3053, Mar. 2010.

[11] “Hypercolor,” 2007. [Online]. Available: http://en.wikipedia.org/wiki/Thermochromism#mediaviewer/File:Generra_Hypercolor_2.jpg. [Accessed: 05-Feb-2015].

[12] P. Brühwiler and M. Buyan, “Facial warming and tinted helmet visors,” *EMPA Act.*, vol. 5, no. February, p. 49, 2005.

[13] “PhotochromicLens,” 2007. [Online]. Available: http://commons.wikimedia.org/wiki/File:PhotochromicLens.jpg. [Accessed: 09-Feb-2015].

[14] H. Manz, S. Brunner, and L. Wullschleger, “Triple vacuum glazing: Heat transfer and basic mechanical design constraints,” *Sol. Energy*, vol. 80, pp. 1632–1642, 2006.

[15] I. P. Parkin and T. D. Manning, “Products of Chemistry Intelligent Thermochromic Windows,” *J. Chem. Educ.*, vol. 83, no. 3, pp. 393–400, 2006.

[16] H.-N. Cui, V. Teixeira, L.-J. Meng, R. Wang, J.-Y. Gao, and E. Fortunato, “Thermochromic properties of vanadium oxide films prepared by dc reactive magnetron sputtering,” *Thin Solid Films*, vol. 516, no. 7, pp. 1484–1488, 2008.

[17] R. Santos, J. Loureiro, a. Nogueira, E. Elangovan, J. V. Pinto, J. P. Veiga, T. Busani, E. Fortunato, R. Martins, and I. Ferreira, “Thermoelectric properties of V2O5 thin films deposited by thermal evaporation,” *Appl. Surf. Sci.*, vol. 282, pp. 590–594, 2013.

[18] J. Loureiro, R. Santos, A. Nogueira, F. Wyczisk, L. Divay, S. Reparaz, F. Alzina, C. M. S. Torres, J. Cuffe, M. F. Montemor, and Others, “Nanostructured p-type Cr/V 2 O 5 thin films with boosted thermoelectric properties,” *J. Mater. Chem. A*, pp. 6456–6462, 2014.

[19] J. W. Lee, I. H. Park, S. Il Cho, C.-R. Cho, and C. W. Chung, “Thin Films,” *Integr. Ferroelectr.*, vol. 80, no. February 2015, pp. 181–188, 2006.

[20] M. E. a Warwick and R. Binions, “Advances in thermochromic vanadium dioxide films,” *J. Mater. Chem. A*, vol. 2, pp. 3275–3292, 2014.

[21] C. G. Granqvist, P. C. Lansåker, N. R. Mlyuka, G. a. Niklasson, and E. Avendaño, “Progress in chromogenics: New results for electrochromic and thermochromic materials and devices,” *Sol. Energy Mater. Sol. Cells*, vol. 93, pp. 2032–2039, 2009.

[22] Z. Zhang, Y. Gao, Z. Chen, J. Du, C. Cao, L. Kang, and H. Luo, “Thermochromic VO2 thin films: solution-based processing, improved optical properties, and lowered phase transformation temperature.,” *Langmuir*, vol. 26, no. 13, pp. 10738–44, Jul. 2010.

[23] Y. Gao, H. Luo, Z. Zhang, L. Kang, Z. Chen, J. Du, M. Kanehira, and C. Cao, “Nanoceramic VO2 thermochromic smart glass: A review on progress in solution processing,” *Nano Energy*, vol. 1, no. 2, pp. 221–246, 2012.

[24] M. Saeli, C. Piccirillo, I. P. Parkin, I. Ridley, and R. Binions, “Nano-composite thermochromic thin films and their application in energy-efficient glazing,” *Sol. Energy Mater. Sol. Cells*, vol. 94, no. 2, pp. 141–151, 2010.

[25] Y. Sun, X. Xiao, G. Xu, G. Dong, G. Chai, H. Zhang, P. Liu, H. Zhu, and Y. Zhan, “Anisotropic vanadium dioxide sculptured thin films with superior thermochromic properties.,” *Sci. Rep.*, vol. 3, p. 2756, 2013.

[26] “SolarSpectrum.” [Online]. Available: http://qdl.scs-inc.us/2ndParty/Pages/10522.html. [Accessed: 11-Feb-2015].

[27] J. H. Son, J. Wei, D. Cobden, G. Cao, and Y. Xia, “Hydrothermal synthesis of monoclinic VO2 micro- and nanocrystals in one step and their use in fabricating inverse opals,” *Chem. Mater.*, vol. 22, no. 10, pp. 3043–3050, 2010.

[28] T. V. O. M, S. R. Popuri, M. Miclau, A. Artemenko, C. Labrugere, and A. Villesuzanne, “Rapid Hydrothermal Synthesis of VO 2 (B) and Its Conversion to,” *Inorg. Chem.*, vol. 2, pp. 4780–4785, 2013.

[29] J. Kirschbrown, “RF/DC Magnetron Sputtering,” *Unc.Edu*, vol. 1, pp. 1–4, 2007.

[30] Luxasolar, “Sputtering,” 2010. [Online]. Available: http://commons.wikimedia.org/wiki/File:Sputtering.jpg. [Accessed: 11-Mar-2015].

[31] J. Livage, “Optical and electrical properties of vanadium oxides synthesized from alkoxides,” *Coord. Chem. Rev.*, vol. 190–192, pp. 391–403, 1999.

[32] R. Eugénio, “Materiais termocrómicos de filme fino,” Master thesis, FCT-UNL, 2013.

[33] P. Auxiliar, “Produção e desenvolvimento de dispositivos baseados em materiais termoeléctricos,” Master thesis, FCT-UNL, 2011.

[34] J. Du, Y. Gao, Z. Chen, L. Kang, Z. Zhang, and H. Luo, “Enhancing thermochromic performance of VO2 films via increased microroughness by phase separation,” *Sol. Energy Mater. Sol. Cells*, vol. 110, pp. 1–7, 2013.

[35] J. Montero, Y.-X. Ji, S.-Y. Li, G. a. Niklasson, and C. G. Granqvist, “Sputter deposition of thermochromic VO2 films on In2O3:Sn, SnO2, and glass: Structure and composition versus oxygen partial pressure,” *J. Vac. Sci. Technol. B, Nanotechnol. Microelectron. Mater. Process. Meas. Phenom.*, vol. 33, no. 3, p. 031805, 2015.

[36] R. E. Marvel, R. R. Harl, V. Craciun, B. R. Rogers, and R. F. Haglund, “Influence of deposition process and substrate on the phase transition of vanadium dioxide thin films,” *Acta Mater.*, vol. 91, pp. 217–226, 2015.

[37] Y. Guo, H. Xu, C. Zou, Z. Yang, B. Tong, J. Yu, Y. Zhang, L. Zhao, and Y. Wang, “Evolution of structure and electrical properties with annealing time in solution-based VO2 thin films,” *J. Alloys Compd.*, vol. 622, pp. 913–917, 2015.

[38] L. Ortega-Reyes and a. Ávila-García, “Thermally grown vanadium oxide films and their electrical properties,” *Mater. Sci. Semicond. Process.*, vol. 37, pp. 123–128, 2015.

[39] “OSB.” [Online]. Available: http://www.jular.pt/conteudos.php?lang=pt&id_menu=20. [Accessed: 03-Jun-2015].

## ANNEX

This section contains all the complementary data acquired throughout experimentation and characterization.

### Annex A

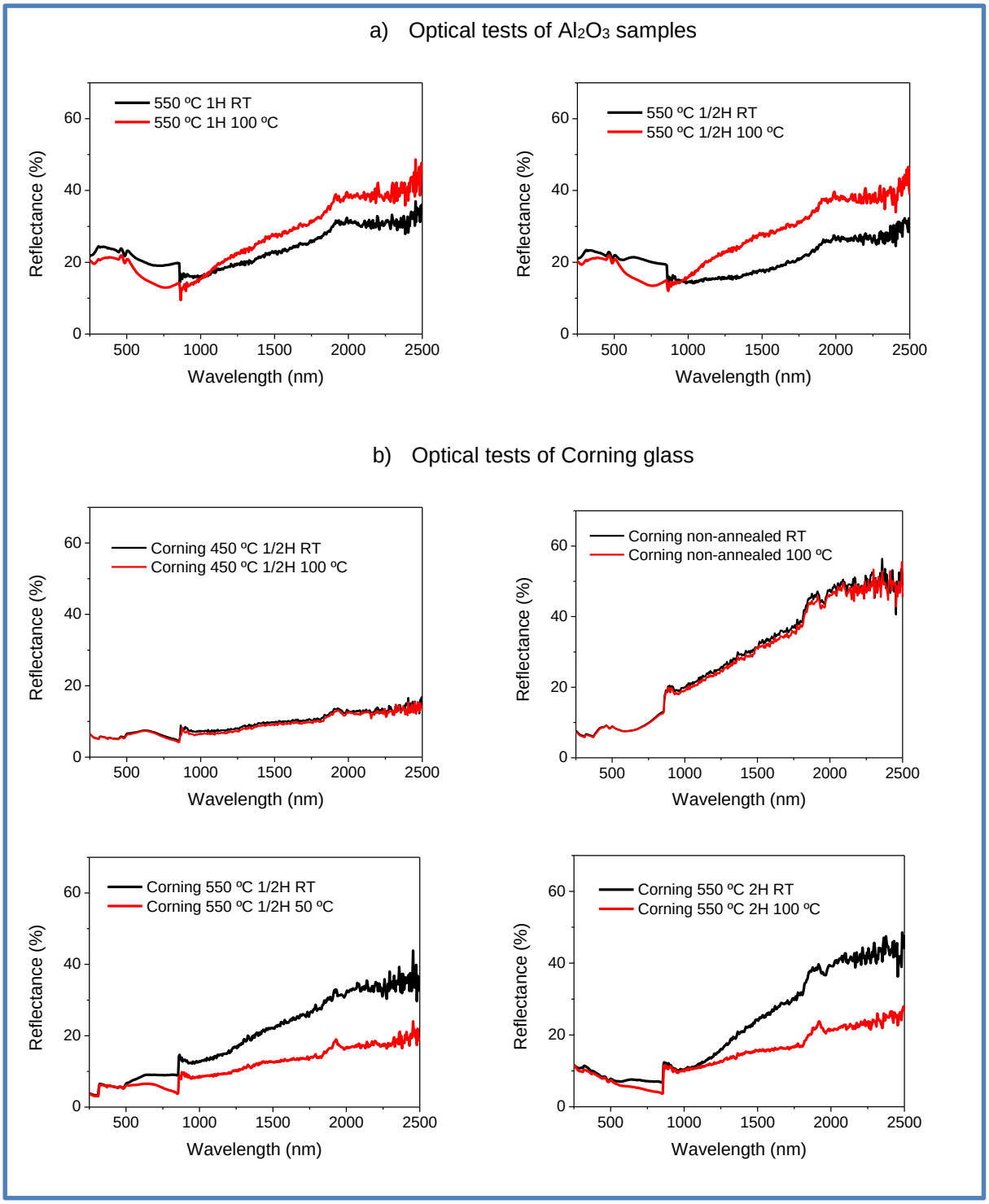


**Figure A.1 – Reflectance spectra of $VO_2$ thin films on $Al_2O_3$ and Corning glass substrates.**

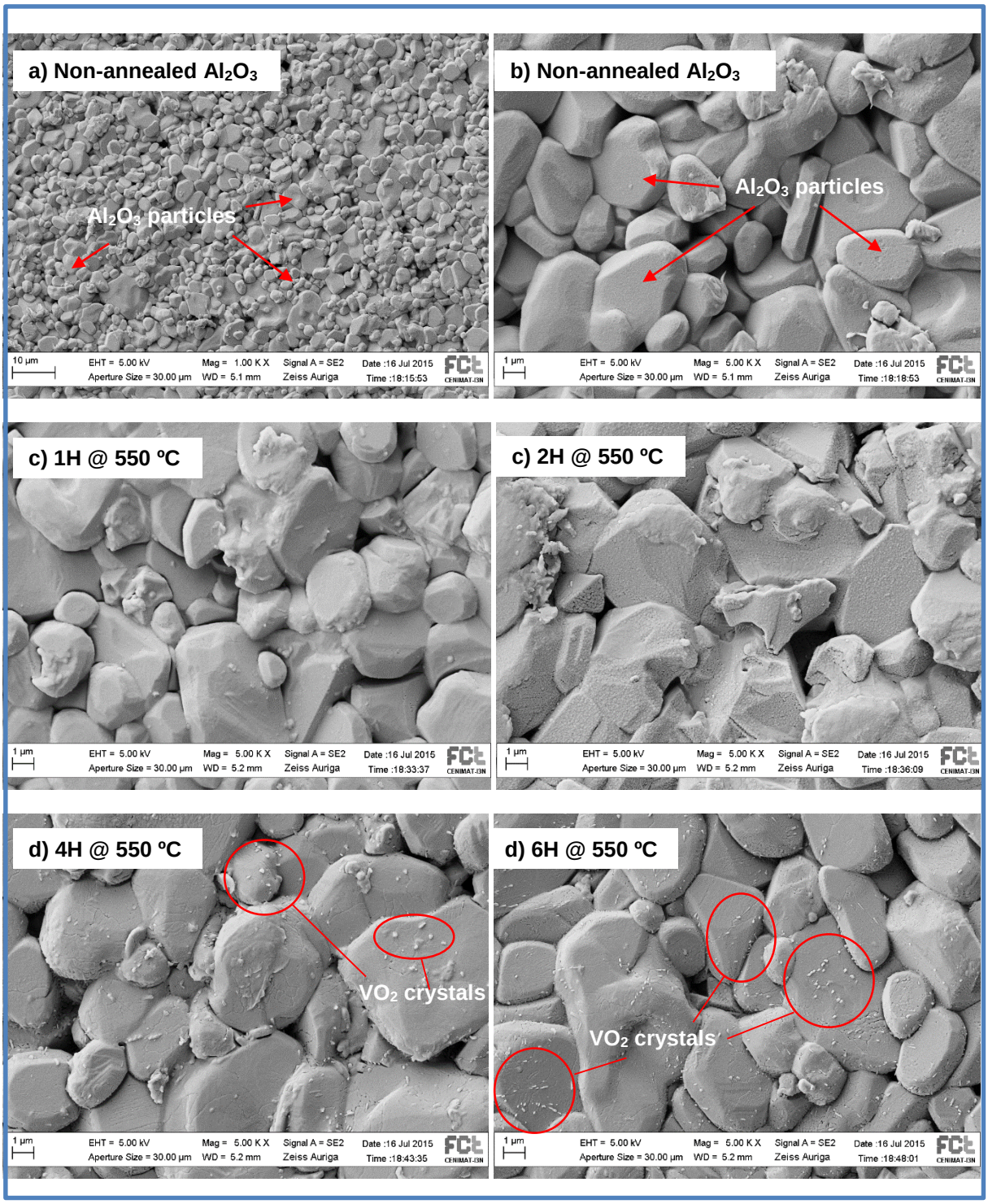


**Figure A.2 - SEM images of $VO_2$ layers deposited on $Al_2O_3$ substrates, with different annealing times.**

## Annex C

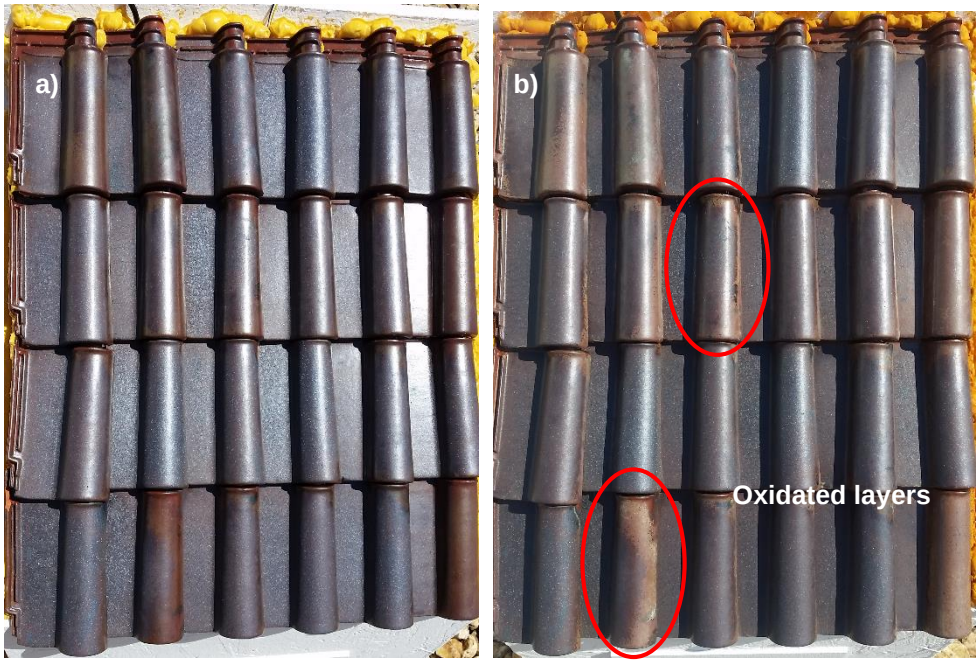


**Figure A.3 - Images of the roof-tiles: one day of exposure (a) and one month exposure (b) to real atmospheric conditions.**

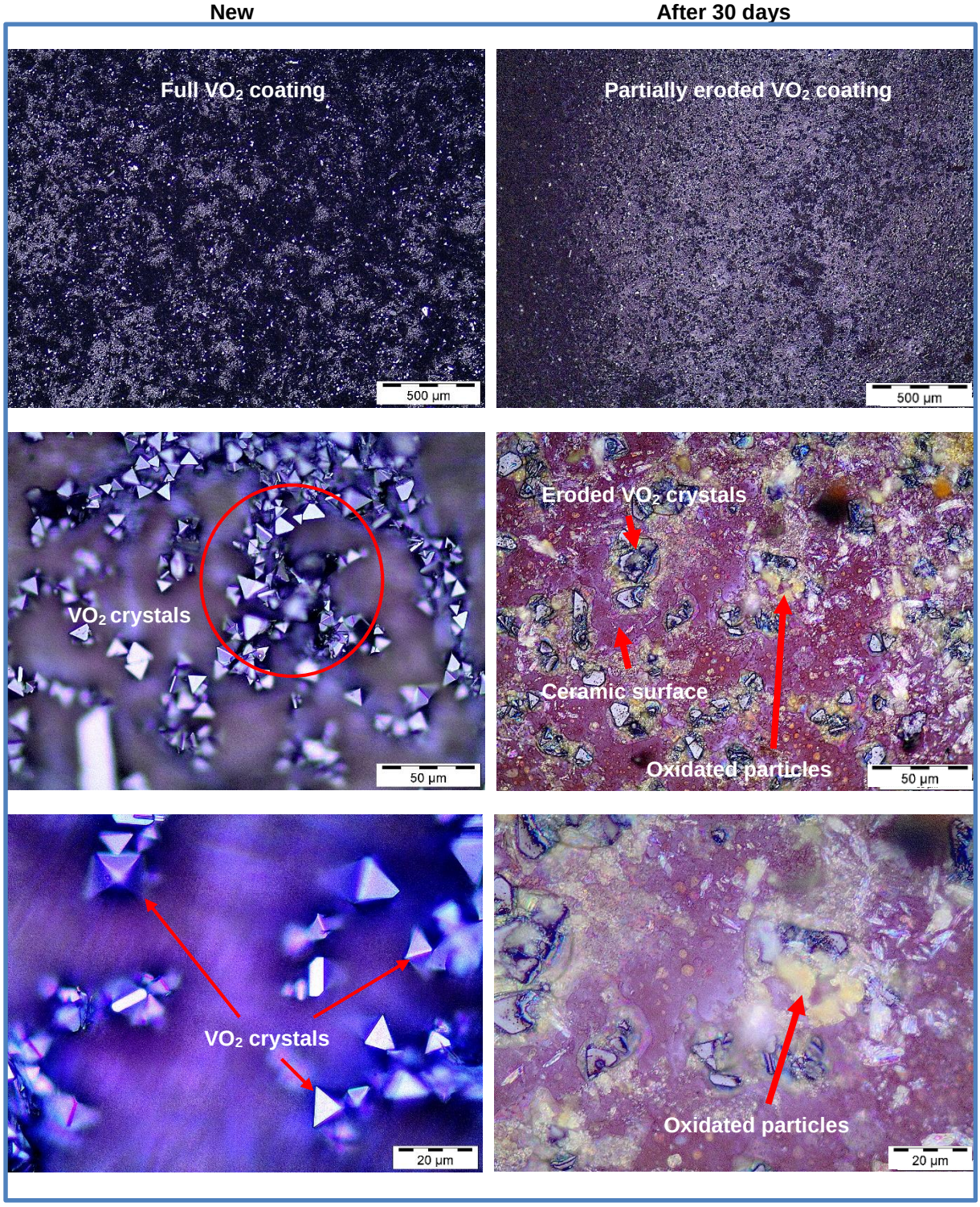


**Figure A.4 - Microscopic images of the $VO_2$ coating of a tile before and after one month exposure to real atmospheric conditions.**